UNCLASSIFIED

AD 273 540

Reproduced
by the

ARMED SERVICES TECHNICAL INFORMATION AGENCY
ARLINGTON HALL STATION
ARLINGTON 12, VIRGINIA

UNCLASSIFIED

NOTICE: When government or other drawings, specifications or other data are used for any purpose other than in connection with a definitely related government procurement operation, the U. S. Government thereby incurs no responsibility, nor any obligation whatsoever; and the fact that the Government may have formulated, furnished, or in any way supplied the said drawings, specifications, or other data is not to be regarded by implication or otherwise as in any manner licensing the holder or any other person or corporation, or conveying any rights or permission to manufacture, use or sell any patented invention that may in any way be related thereto.

AD No. 273540
ASTIA FILE COPY
273 540

Copy No. _____

116 400

FILE COPY
Return to
ASTIA
ARLINGTON HALL STATION
ARLINGTON 12, VIRGINIA
Attn: TIRS

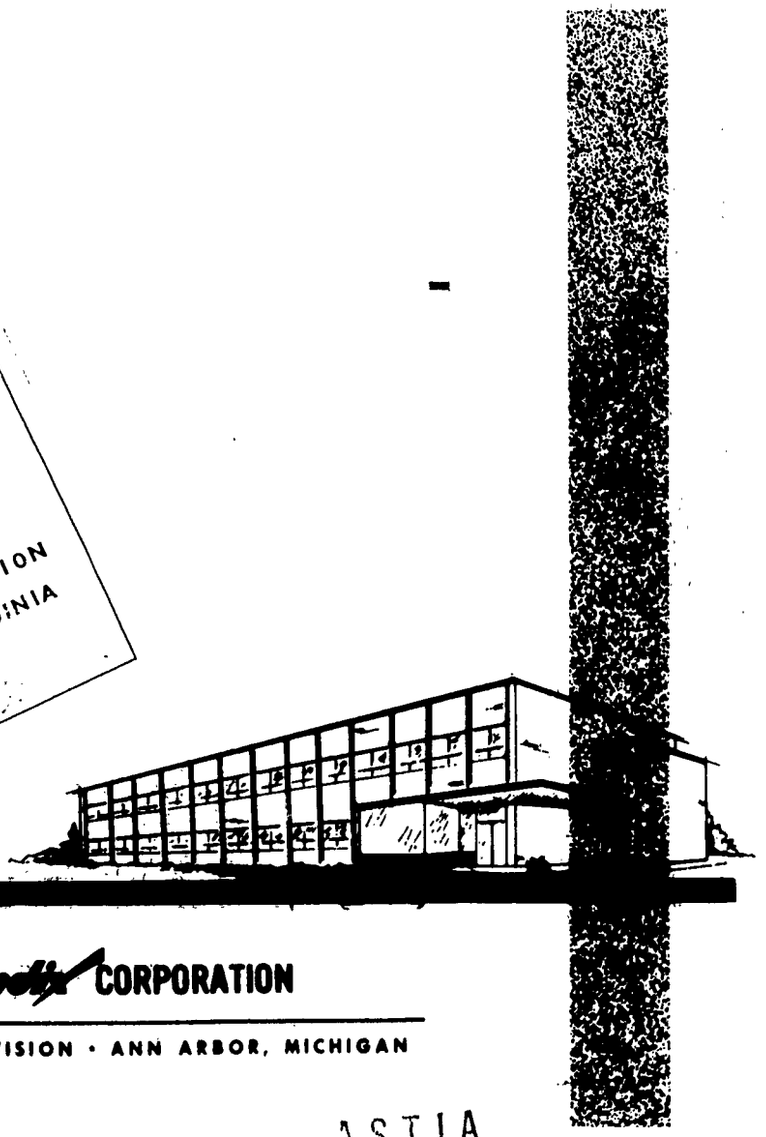

THE Bendix CORPORATION

BENDIX SYSTEMS DIVISION • ANN ARBOR, MICHIGAN

ASTIA
RECEIVED
MAR 28 1962
TISIA
A

$7.60

✓BSC-29556

FS-62TN-1025

LABORATORY PROCEDURES ION AUGMENTATION EXPERIMENTS

Prepared by:
A. O. Kresse
P. J. Doody

February 9, 1962

The work described in this Technical Note was supported by the Department of the Air Force, Contract No. AF 04(694)-26

J. Rutkowski, Dept. Manager

BENDIX SYSTEMS DIVISION
OF
THE BENDIX CORPORATION
Ann Arbor, Michigan

TABLE OF CONTENTS

		Page
1. INTRODUCTION		1
2. PLANNED EXPERIMENTS		1
APPENDIX A	RESOLUTION CELL	17
APPENDIX B	CALIBRATION PROCEDURES	20
APPENDIX C	MEASUREMENT OF ION DENSITIES USING THE HOLTZMARK THEORY OF LINE BROADENING	33
APPENDIX D	ALTERNATE METHOD OF ION DENSITY MEASUREMENT	44
APPENDIX E	OPTICAL METHODS OF TEMPERATURE DETERMINATION	47
APPENDIX F	DETERMINATION OF RADIATING SPECIE CONCENTRATIONS BY A NUMERICAL SOLUTION OF ABEL'S INTEGRAL EQUATION	52
APPENDIX G	BOUNDARY LAYER VELOCITY PROFILE	55
APPENDIX H	CHEMICAL REACTIONS, RATE EQUATIONS, AND REACTION RATE CONSTANTS FOR KINETICS STUDY	58
APPENDIX I	ANALYSIS OF RADIATION FOR CHEMICAL RATE DATA	63
APPENDIX J	PHYSICAL DATA	67

LIST OF ILLUSTRATIONS

Figure	Title	Page
1	General Equipment Layout	2
2	Specific Rocket Nozzle Geometry	4
3	Adjustment of Station 0.0 to Eliminate Nozzle From Field of View	8
4	Configurations for Tests	9
5	Ablation Experiment Setup	11
6	Schematic of Flow System for Kinetics Experiment	14
A-1	Resolution Cell Diagram	18
B-1	Spectral Radiance Versus Wavelength for Two Source Temperatures	21
B-2	Filament Characteristics	21
B-3	Outputs of Lamps With Different Effective Source Areas But At Equal Temperatures	23
B-4	Ebert Optics	24
B-5	Wadsworth Optics	27
B-6	Wavelength Marker	27
B-7	Characteristic Curve	29
B-8	Emulsion Characteristics	30
B-9	Stepped Sector	31
C-1	Theoretical Profile H_α	36
C-2	Theoretical Profile H_β	37
C-3	Theoretical Profile H_γ	38
C-4	Theoretical H_α Relative Intensities	39
C-5	Theoretical H_β Relative Intensities	40
C-6	Experimental H_α Line Profile	41
C-7	Experimental H_β Line Profiles	42
D-1	Schematic of a Spectral Line	45
F-1	Concentration Determination	53

LABORATORY PROCEDURES

ION AUGMENTATION EXPERIMENTS

~~1. Introduction~~

~~This technical note presents the specific [illegible] from~~ the conduct of the experimental analysis of electron seeding techniques ~~as required by Contract No. AF 04(694)-26. The purpose of the notes~~ described. to clarify the experimental techniques and to detail the mathematical procedures necessary for analysis and interpretation of the data.

The basic purpose of the experiments is twofold: first, quantitative empirical definition of the performance of electron augmenters, both ablative and rocket motor types, when subjected to a range of conditions which will affect their performance; second, an estimate of the important processes and their rates which determine the rate of electron disappearance in flow subsequent to their generation.

2. Planned Experiments

* The purpose of this presentation is

Rocket motor augmentation, ablation augmentation, and chemical kinetics experiments are currently planned. The first two sets of experiments are called for in the current Bendix Program Plan. The third, while not specifically required, is considered necessary for an accurate estimate of electron depletion rates due to a paucity of available data.

2.1 Rocket Motor Experiment

The basic purpose of the rocket motor experiment is to determine the empirical electron flow rate from the nozzle exit plane for a specific rocket motor design.

2.1.1 Vacuum Chamber Operation

The rocket motor will be operated in the vacuum system as shown in Figure 1 at exhaust pressures corresponding to altitudes of 100, 175, and 225 kilofeet altitude (8.29 mm Hg., 0.443 mm Hg., 0.0586 mm Hg., respectively). These pressures are nominal settings prior to the run. Variations of $\pm$ 10% are acceptable. The actual pressure during rocket operation is to be recorded continuously.

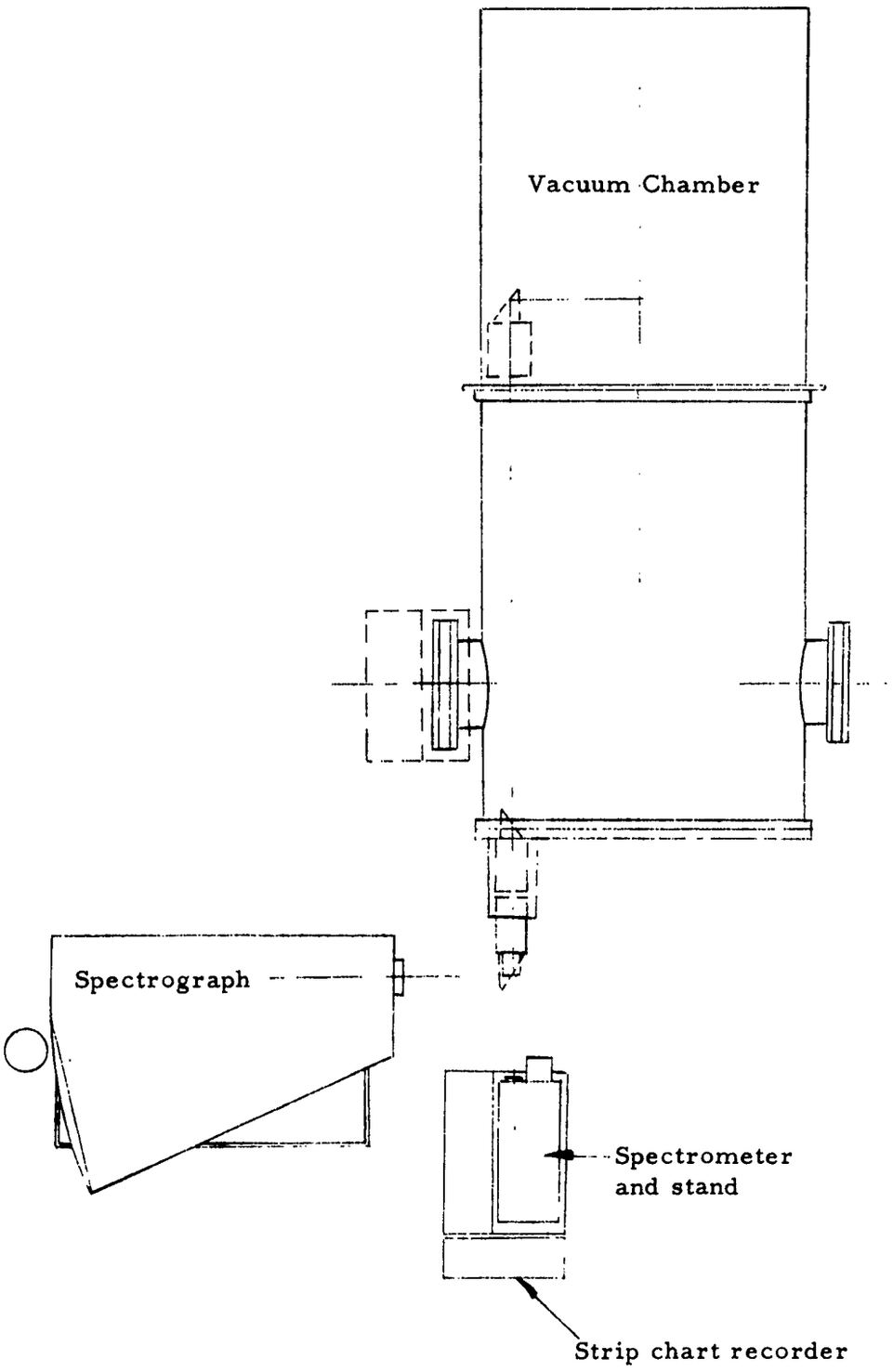

Figure 1: General Equipment Layout

2.1.2 Rocket Motor Ballistics

The rocket motor will be run according to the procedures set up by the Atlantic Research Corp. Pressure and temperature will be recorded continuously via the pressure sensors and thermocouples provided. The weights of active components (propellant, igniter, and insulator) shall be measured before and after each run and the average mass flow of each determined from the running time.

For each altitude the nozzle shall be nominally correctly expanded based on estimated frozen gas properties and nominal chamber pressure. Although it would be desirable to have uniform parallel flow at the nozzle exit, the uncertainties in the pressure and various gas properties do not make it practical to design such a nozzle. The specific nozzle geometries are shown in Figure 2.

2.1.3 Spectrographic Measurements

All of the thermodynamic and physical measurements made on the gas after it leaves the nozzle exit are spectrographic. The layout of the optical train is shown in Figure 1.

The optical system as shown images the entrance slit of the spectrograph to the vertical plane passing through the center line of the jet. The vertical position of the slit may be varied to obtain radial variation of intensity.

Since the optical system is stigmatic there is a defined "resolution cell" from which all radiation reaching the detector comes. The geometry of the cell is analyzed in Appendix A. The optical system and the detector of the spectrograph are calibrated on an absolute intensity basis against a National Bureau of Standards ribbon filament lamp. The calibration procedures and data are described in Appendix B.

The basic output of the instrumentation is the radiant energy from the resolution cell in ergs per volume of the cell per spherical solid angle. The solid angle is defined by the effective "f" number of the optics per wavelength interval and the effective wavelength interval is in turn determined by the spectrograph dispersion and effective slit width.

Pressure	Length	Diameter
8.29 mm	1.26"	1.174"
0.40 mm	4.85"	4.52"
0.06 mm	12.25"	11.4"

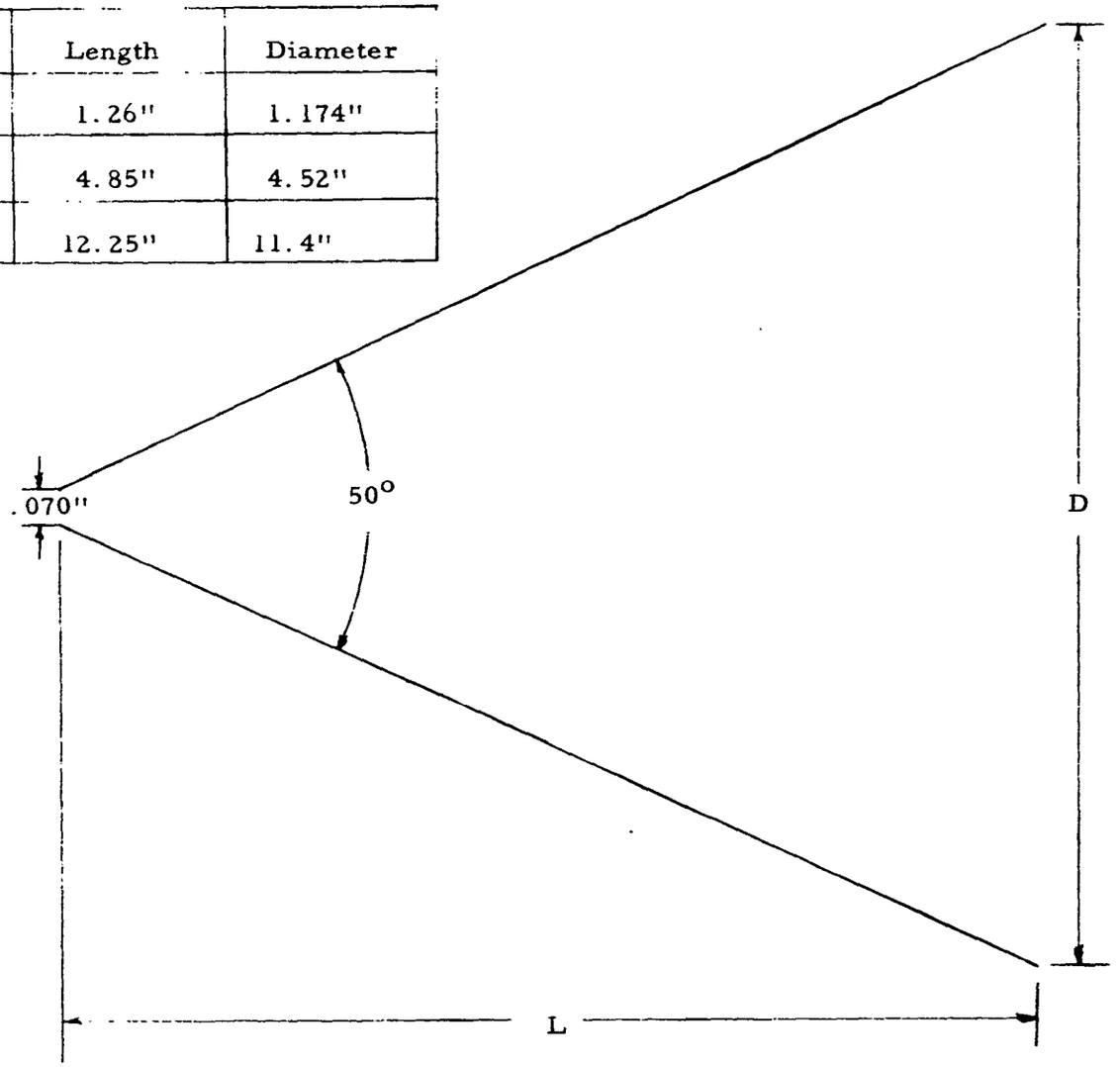

Figure 2: Specific Rocket Nozzle Geometry

The corrected data is of the form:

$$I_{corr} = \frac{\text{ergs}}{\text{cm}^3,\ \text{steradian},\ \text{Å},\ \text{sec}}$$

over the range of wavelengths and spatial extent desired. The fundamental equation for specie density used in the quantitative spectral analysis is

$$4\pi \int_{-\Delta\lambda}^{\Delta\lambda} I_{corr}\ d\lambda = N_i\, g_i\, A_{ij}\, N\, \nu_{ij}\ \left(\frac{\text{ergs}}{\text{sec}}\right) \qquad (1)$$

where the integral is taken over the whole line of a particular transition N_i is the number density in the upper energy state i, g_i is the degeneracy of the upper state, A_{ij} is the transition probability from state i to state j, and $h\nu_{ij}$ is the energy of a single transition from state i to state j. The number of interest is N_i which is the only unknown quantity in the equation. The other factors are either measured or known beforehand. The basic assumption made in the derivation of Equation (1) is that self absorbtion is negligible, an assumption that improves as the density is decreased and is valid for practical purposes over the range of density to be encountered in this experiment. The major difficulty expected in the analysis of the data is to resolve the line of interest from the background. In principle, the total density of a given specie in a gas sample is obtained simply by summing the N_i determined by Equation (1). In practice, however, not all transitions are accessible to the spectrograph due either to insufficient intensity or wavelengths out of the band pass of the instrument. If the interval states of a given specie are in equilibrium then Boltzmann's distribution law applies and the number density may be parameterized in terms of a "temperature" and the missing elements in the sum determined. The applicable form of Boltzmann's law is:

$$N_i = \frac{g_i\, e^{-\frac{\epsilon_i}{kT}}}{\sum_i g_i\, e^{-\epsilon_i/kT}}\ N \qquad (2)$$

The denominator of Equation (2) is the partition function, and for the range of temperatures considered here is roughly constant. In fact, little accuracy is lost in calling it constant for this calculation. If greater accuracy is necessary, one or two iterations will yield the correct value. Thus calling:

$$\sum g_i \; e^{-\epsilon_i / kT} = Q = \text{constant (from the experimental data)}$$

we may plot

$$k \ln \frac{N_i \, Q}{g_i} = -\epsilon_i \frac{1}{T} \qquad (3)$$

versus ϵ_i which will be a straight line with slope $-\frac{1}{T}$ if the assumption of internal equilibrium is correct. The parameter T so determined may then be used to calculate the inaccessible N_i's and the total specie density determined as

$$N_s = \sum_{o}^{\infty} N_{s_i}$$

where "s" refers to s^{th} specie. In practice because of the exponential form of the population equation the infinite sum is not required (or possible) and the sum may be truncated at a few terms.

It should be noted that the parameter T should in no case be interpreted as the local kinetic temperature unless it is determined by other means that local thermodynamic equilibrium prevails.

The method described above for specie density measurement is quite general although most conveniently applied to atomic species with well separated lines. For molecular species it is more convenient to deal with integrated vibrational band intensities of the individual electronic states. Since Cs and Cs^+ are the most important species from the standpoint of electron generation and depletion, the experimental measurements will be confined to them unless experience shows that other molecular and atomic species are playing an important role.

The most interesting specie from the standpoint of program objective is, of course, the electrons. The preceding methods are not applicable to measurement of electron densities and other techniques must be found.

The general method involves the measurement of line shapes which can, by various theoretical methods, be related to the ion and/or electron density, Note that it is always assumed here that the ion and electron densities are equal. The details of the analytical procedures are given in Appendices (C) and (D). Since the spectrograph is assumed to have been calibrated absolutely, a single spectral measurement is sufficient for both types of analyses, although for the electron density measurements only a relative calibration is required and then only to ensure that no detector response anomalies exist in the vicinity of the line in question. This is so since only the relative line shape is important.

The measurements of most significance are those at the exit plane of the nozzle since it is only there that there is a reasonably good knowledge of the flow velocity and temperature. Downstream of the nozzle, diffusion and mixing gradually destroy the homogeneous character of the stream and although the measurements can be made their interpretation in terms of rate processes becomes less and less meaningful.

A tentative selection of axial stations in terms of nozzle exit diameters (which will vary with design exit pressure) is 0.0, 0.5, 1.0, 3.0, and 5.0 diameters.

It should be noted that the 0.0 station is nominal. The actual position of the slit image should be such that no part of the nozzle wall is seen by the optical system as shown in Figure 3. This position must be found by trial and error. The temporal sequence of the measurements should be from station 0.0 to downstream since the limited running time may preclude the last measurement. The initial runs are to be made with the optical axis of the instrument intersecting the center line of the jet (Figure 4). The analysis is to be carried out assuming no radial gradients in gas properties. If time permits, this assumption will be checked by making measurements with the slit displaced toward the edge of the jet.

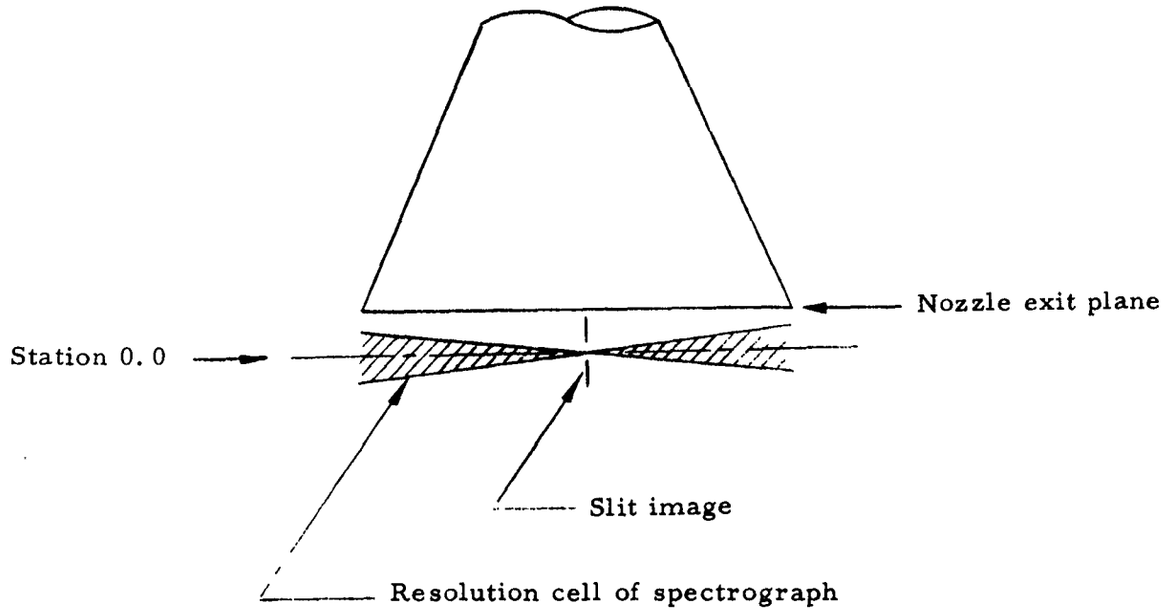

Figure 3 Adjustment of Station 0.0 To Eliminate Nozzle From Field of View

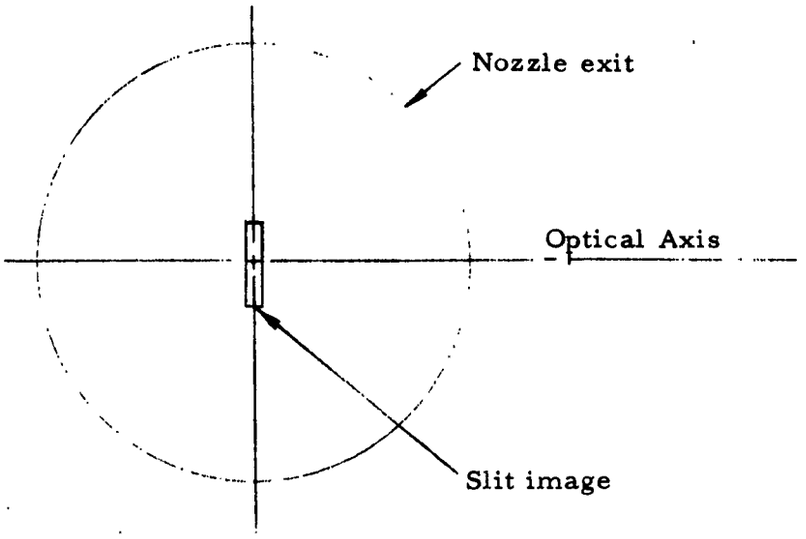

Configuration for Initial Tests

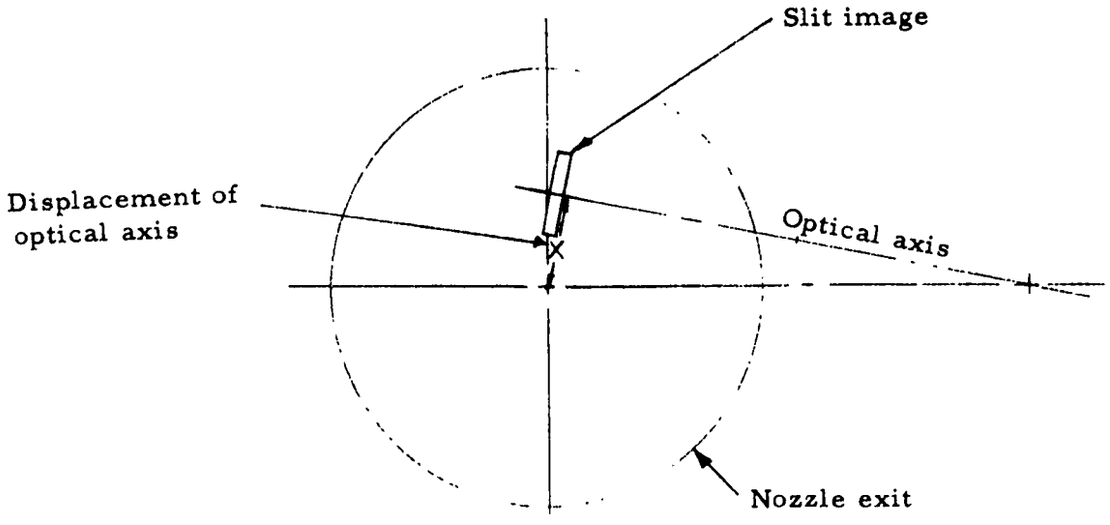

Configuration for Supporting Tests

Figure 4: Configurations for Tests

2.2 Ablation Experiments

The basic measurements to be performed in the ablation tests are similar in nature to those of the rocket motor tests and will not be re-described here. The differences lie largely in the experimental geometry and the source of the electrons. The setup is shown in Figure 5. The test gas (which may be anything required for the purpose of the experiment) is heated in the arc chamber, allowed to equilibrate in the setting chamber, and then correctly expanded to the desired free stream conditions which are the same as in the previous experiment.

The ablation sample, which ordinarily will be a pointed rod of carbon infiltrated with a seeding material, is to be placed a short convenient distance from the nozzle exit plane.

An attached weak shock will develop at the tip of the rod and at the shoulder the expansion fan will re-expand the gas to free stream pressure. It is assumed that because of the weak shock the flow is nearly isentropic and the free stream temperature also returns to its initial value (note that the essentially non isentropic flow can be calculated if necessary, particularly if blunt samples are employed). The boundary layer will form on the surface of the rod and grow in thickness down the rod. Conditions in the boundary layer are the prime object of this series of measurements.

In Figure 5 the slit image is shown sitting on top of the rod, slightly overlapping the rod proper. This arrangement implies the use of the photographic instrument since the spectrum is resolved along the slit. The lower protion of the spectrum is then the black body radiation from the surface on which is superimposed the local gaseous radiation. The upper part of the spectrum contains the radiation from the boundary layer which is in the region of strong gradients. From the black body radiation the surface temperature of the rod may be determined directly by noting the wavelength of peak intensity if it is in the sensible range of the spectrograph, or by a slightly more complicated two color analysis (Appendix E).

Since the discrete spectrum is from a region of strong gradients the radial variation of intensity must be determined by a numerical solution of Abel's integral equation (Appendix F). Once the radial grandients have been determined the specie densities and temperatures may be calculated as before.

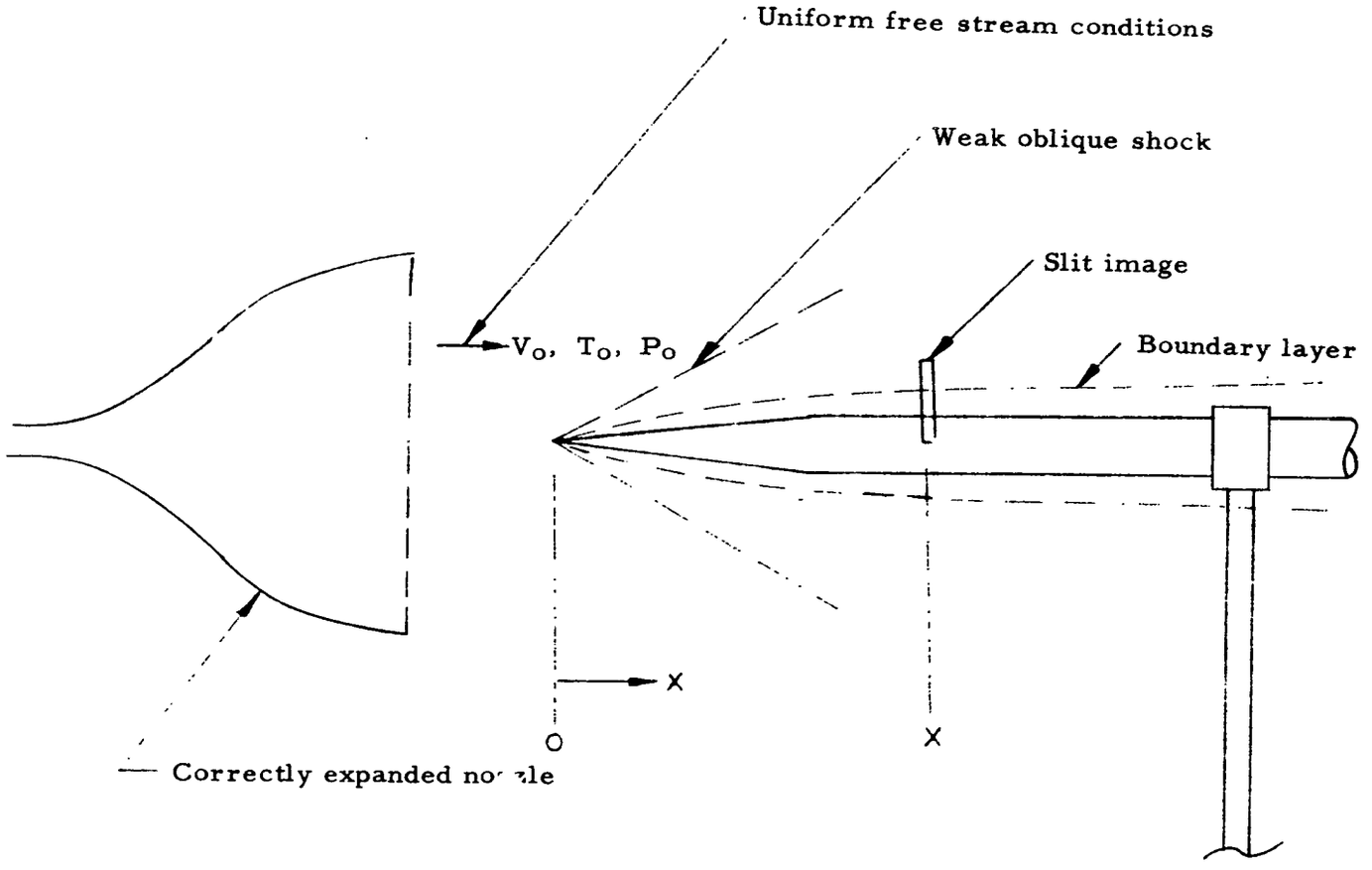

Figure 5: Ablation Experiment Setup

The actual flux rates of electrons from the surface must be determined from an a priori estimate of local velocities since under the conditions of the experiment the boundary layer velocity distributions cannot be measured. The thermal thickness can be measured, however, which is of considerable help. The basic boundary layer equations to be used are given in Appendix G.

Since the photographic instrument does not resolve time, the light beam from the gas will be split, half going to the photographic instrument and half to the recording monochromator which will be set to cover a line of particular interest, e.g., a strong Cs or Cs^+ line. In this way the relative evolution rate may be traced and the photographic data taken at the most opportune moment. This is important since the samples have a surface layer of pure seeding material which will flash at the start of a run. After the flash a steady evolution of material occurs due to ablation and it is during this latter period that the quantitative data must be taken.

The axial position (x) of the measurements is yet to be determined precisely and, since there are fairly strong axial temperature gradients in the carbon rod, the measurement stations must be chosen with care. The three most likely places are cone midpoint, just aft of the cone shoulder, and a far downstream point where the rod is relatively cool. A standard set of locations will be selected, however, in order to compare the data empirically.

The ablation samples to be tested initially are 1/2" diameter carbon rods which have been vacuum impregnated with materials or compounds of materials which are known to have a low ionization potential. These are aluminum, sodium, potassium nitrate and cesium nitrate. The reasons for selecting the salts of cesium and potassium are to minimize the handling hazards and to eliminate the formation of alkali carbides which have little or no mechanical strength.

Since the total amount of impregnated material is known, a rough estimate of the material lost will be obtained by weighing the sample after a run, assuming that no carbon is lost. A quantitative chemical analysis of the ablated sample will give better results and will be performed if techniques are available. (American Metal Products made the original samples and will be sent the used samples for chemical analysis.)

2.3 Kinetics Experiment

The kinetics experiment as described below differs from the preceding experiments in that the desired data is quantitative chemical rate data rather than a demonstration of feasibility. Also, the experimental setup only grossly simulates the augmenter device. Indeed, the similarity is accidental rather than necessary.

The basic problem of a kinetics experiment is the temporal resolution of time-dependent events. The means by which time resolution is provided depends largely on the time scale of the process being investigated. For the case of reactions at high temperatures, such as those considered here, the time scale is of the order of 10^{-6} to 10^{-4} seconds. Such short times preclude the investigation of a homogeneous reaction in a closed vessel or slow flowing gases in ducts. Residence times of the order of 10 to 100 microseconds are conveniently obtained in DeLaval nozzles. Furthermore, when the sample gas is heated by an electric arc, the initial conditions of temperature, enthalpy and pressure are controllable at will and are not dependent upon the chemical heat release. It is for these reasons that the supersonic flow in a nozzle has been chosen as the time resolution mechanism for these kinetic experiments. The basic apparatus is shown in a schematic form in Figure 6. The general method of operation is as follows:

Argon (or other gases if desired) is injected into the arc chamber at rates consistent with good operating conditions for the arc. The arc is struck and the gas is heated to some stagnation temperature equal to or greater than the desired value. Because of the nature of arc processes the resulting hot gas is in a highly non-equilibrium state. The gas then flows to the settling chamber where the long residence times allow equilibration to occur. If necessary, additional cold gas may be injected here to reduce the stagnation temperature to the desired value.

At this time the chemical system under consideration is also injected, in this case $CsNO_3$ and Al. The quantities are so selected to make the total heat of the reaction insignificant compared to the enthalpy of the diluent. This allows one to ignore the reaction thermodynamically and compute local temperatures and pressures based upon the diluent properties only. This latter is not essential to the experiment but the simplication in the analysis is considerable.

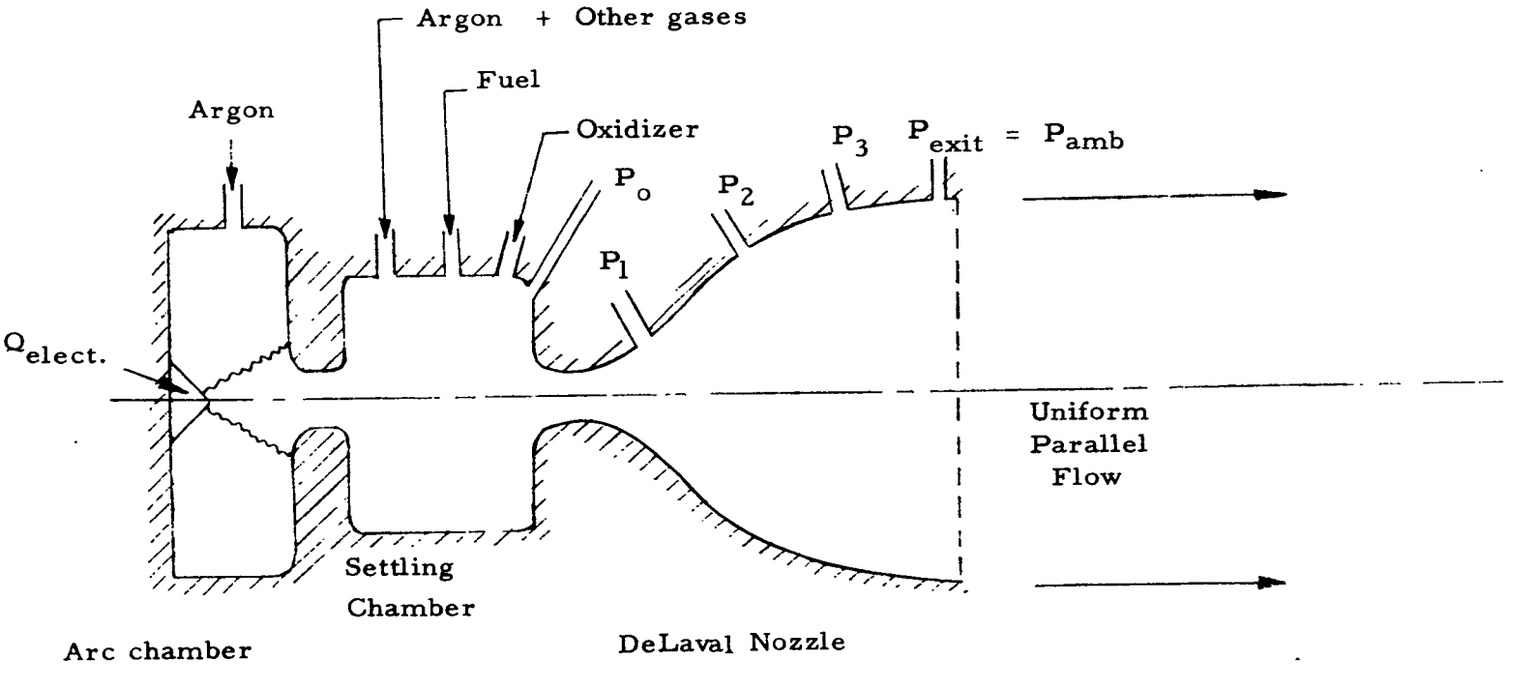

Figure 6

Schematic of Flow System
For Kinetics Experiment

Because of the complexity and number of possible reactions which can occur with the reactants selected, it is desirable to sort out empirically the dominant reactions. The procedure for doing this is to vary the concentrations of species independently of what is obtained from the initial reactants. All atomic species except Cs can be varied at will by mixing with the prime gas. The various percentages which will be added cannot be pre-estimated specifically but factors of 2 or 3 are centainly reasonable. The system of chemical and rate equations along with present estimates of the rate constants are given in Appendix I.

The most interesting ones are, of course, those which involve electrons. The equations which do not involve electrons are present because they form part of the chain which supply atomic and molecular species appearing in the electron reactions. The specie concentration measurement will be made in the same manner as described for the first experiment. The method of analysis for simple reactions is described in Reference 2 and repeated in Appendix H. A similar method will be used to obtain a global electron recombination rate for the more complicated set of reactions involved in the present process. Because of the complexity, the results will most probably show a non-integral order and will be strictly applicable only to the conditions of the test. The test conditions of Reference 2 permitted the use of glass-walled nozzles and thus only a single nozzle was required. For the present tests, transparent walls do not appear practical. To trace the composition as a function of position in the nozzle, a series of nozzles will be used, each having a different residence time. Since the exit velocity is only a slowly varying function of pressure ratio for very large ratios, it follows that the residence time is predominantly a function of nozzle length. For this reason, it appears simple to fix pressure ratio and vary the residence time by varying length only, such that the area is a common function of the non-dimensional axial position ($\bar{x} = X/L_o$) where L_o is the nozzle length, i. e., a nozzle which "stretches" in the x direction only. Therefore, the time to attain any pressure and temperature in the nozzle will scale directly as the length. Also, a single equilibrium and frozen calculation will suffice for any given set of initial conditions. The method of analysis for the more complicated case is presently being developed.

References

1) Penner, S. S.; Quantitative Molecular Spectroscopy and Gas Emissivities; Addison-Wesley; Reading, Mass.; 1959.

2) Wegener, P. P.; Phys. Fluids 2, 264 (1959).

APPENDIX A

RESOLUTION CELL

It is desirable to define the resolution cell of plasma referred to the optical system used in the experiment. The system is arranged as in Figure A-1, where the single lens shown represents the combined optical system.

Cylindrical symmetry is assumed for the plasma, and the radiation density is assumed to be a function of the radial distance, r, from the axis of symmetry. The analysis assumes a cylindrical slab of plasma of thickness h, where h is a characteristic dimension of the spectrograph slit.

Assuming a radiation density variation with radial distance only, the radiation emitted by the incremental volume is given by

$$dI = I(r)\, dV$$

$$= I(r)\, dr\, dA$$

$$= I(r)\, dr\, (hr\, d\theta)$$

The incremental solid angle subtended by the radiating volume, per unit slit area δA, is given by

$$d(\omega) = \frac{dA}{\delta A}$$

$$= \frac{hr\, d\theta}{\delta A}$$

Before performing the indicated integration over θ, the expression for that half of the resolution cell lying between the slit image and the optics will be shown to be the same as that already derived. This conclusion is based on the symmetry of the system and follows from the fact that light entering the optical system is treated as though it had first passed through the slit .[A-1] The foregoing development is reversed, but the same incremental quantities are involved.

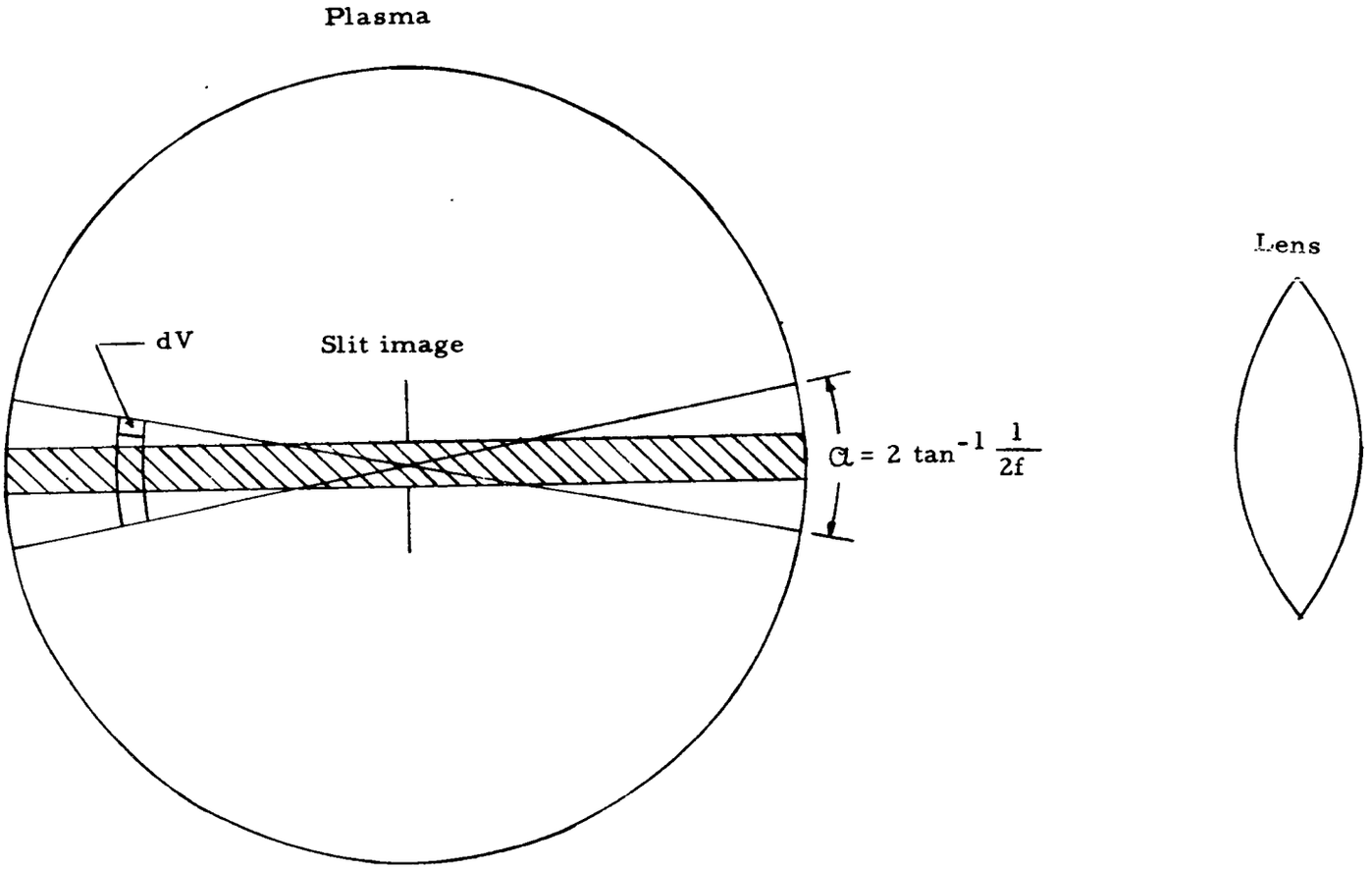

Figure A-1: Resolution Cell Diagram

Now, performing the integration

$$\delta I = \int dI = I(r)\, dr\, (hr\alpha)$$

and

$$\delta \omega = \int d\omega = \frac{1}{\delta A}\, (hr\alpha)$$

so that

$$\frac{\delta I}{\delta \omega} = I(r)\, \delta A\, dr$$

Thus, it is seen that each quasi-annular increment of the resolution cell is equivalent to an incremental volume of cross-section equal to the slit area, having the same radial variation in radiation density.

REFERENCES

A-1 Jenkins, F.A. and White, H.E., Fundamentals of Optics; McGraw-Hill; New York; 1950.

APPENDIX B

CALIBRATION PROCEDURES

I. Calibration of Working Lamps

Tungsten lamps are available which have been calibrated for spectral radiant intensity (watts/steradian) at specified currents, by the National Bureau of Standards. The tungsten lamp, which is very nearly a blackbody radiator, operates at a temperature which depends upon the resistance of the ribbon filament and the current passing through the filament. Due to boiling away of the tungsten filament and subsequent increase in filament resistance and coating of the lamp inner surface, the spectral radiant intensities of the standard lamps decrease as the lamps are used. Unfortunately, the high cost of National Bureau of Standards calibrated lamps makes their use as "working" standards undesirable. However, by using the known characteristics of the N. B. S. calibrated lamps, the spectral radiant intensity of any tungsten lamp may be determined. (It is important that the lamps be of identical composition in order that the grey body emissivities of the filaments and the transmission of the lamp materials be identical.)

According to Planck's law of radiation, the relative wavelength distribution of radiant flux depends only upon the temperature of the emitter (see Figure B-1). Also, Wein's displacement law states that the wavelength of the maximum radiance varies inversely with temperature (also Figure B-1). Thus, for tungsten filaments at the same temperature, the relative radiant intensity curves (normalized to a given wavelength) will be identical. It remains then to determine the constant of proportionality which exists between the outputs of the NBS lamp and the working lamp.

Determination of Filament Temperature

For a given lamp, the filament temperature is a function of the current, the dependency being determined in the laboratory by finding the location of the radiant intensity maxima at various currents and applying Wein's displacement law. That one has determined an actual radiant intensity maximum rather than the maximum sensitivity point of the measuring device may be checked by calibrating the measuring device (sensitivity as a function of wavelength) using the NBS lamp and the known data for that lamp. Then, as shown by the dashed lines in Figure B-2, it is a simple matter to determine the desired operating current for the working lamp.

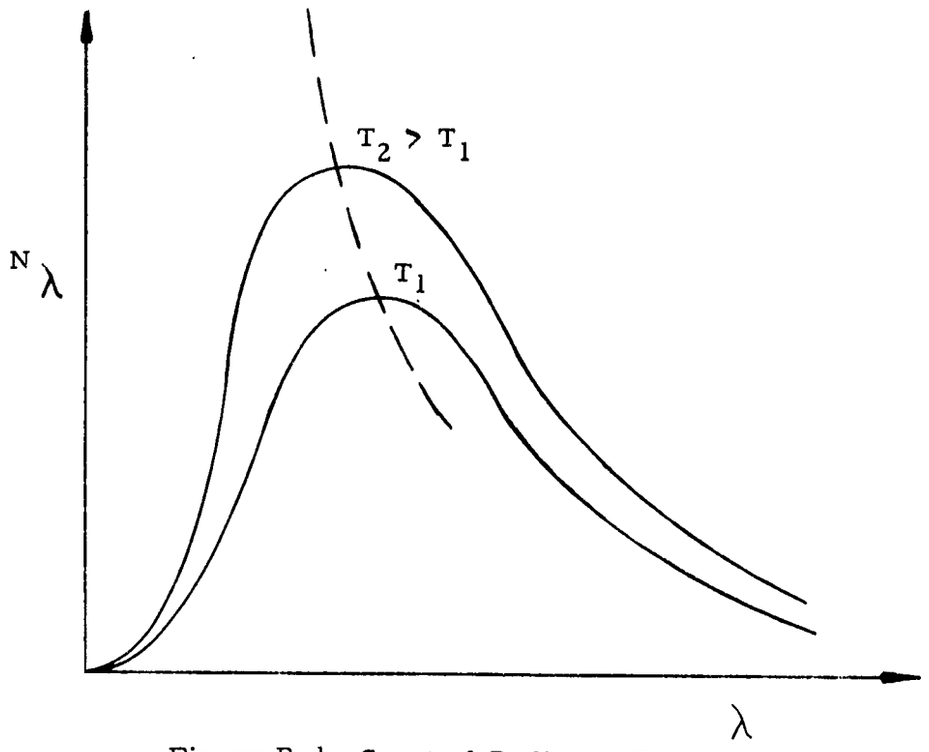

Figure B-1: Spectral Radiance Versus Wavelength for Two Source Temperatures

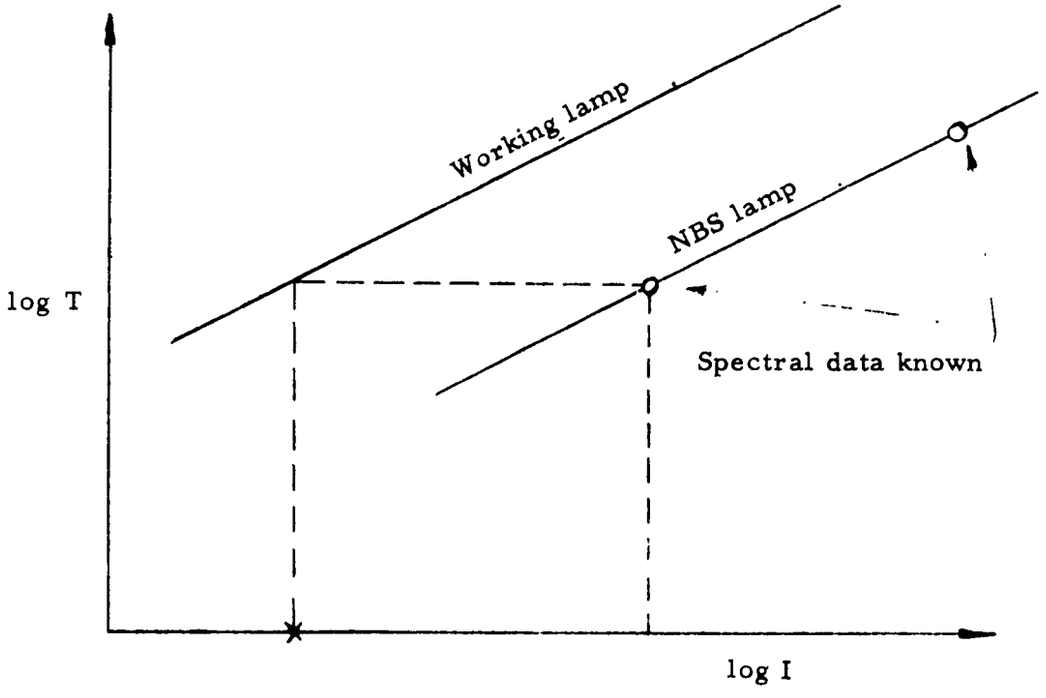

Figure B-2: Filament Characteristics

J. - A. Recording System Attenuation Table

Step Number		Final Attenuation Switch Position										
		1	2	3	4	5	6	7	8	9	10	11
Initial Attenuation Switch Position	1		4.935-1	1.995-1	1.007-1	5.097-2	2.074-2	1.058-2	5.364-3	2.183-3	1.113-3	5.678-4
	2	2.027+0		4.042-1	2.041-1	1.033-1	4.204-2	2.144-2	1.087-2	4.424-3	2.256-3	1.151-3
	3	5.014	2.474		5.050-1	2.555-1	1.040-1	5.304-2	2.689-2	1.094-2	5.582-3	2.847-3
	4	9.928	4.899	1.980		5.060-1	2.059-1	1.050-1	5.325-2	2.167-2	1.105-2	5.637-3
	5	1.962+1	9.682	3.193	1.976		4.070-1	2.076-1	1.052-1	4.283-2	2.184-2	1.114-2
	6	4.821+1	2.379+1	9.615	4.856	2.457		5.100-1	2.586-1	1.052-1	5.367-2	2.737-2
	7	9.452+1	4.664+1	1.885+1	9.521	4.818	1.961		5.070-1	2.064-1	1.052-1	5.367-2
	8	1.864+2	9.200+1	3.719+1	1.878+1	9.502	3.867	1.972		4.070-1	2.076-1	1.059-1
	9	4.581+2	2.260+2	9.137+1	4.614+1	2.335+1	9.502	4.846	2.457		5.100-1	2.601-1
	10	8.982+2	4.432+2	1.792+2	9.047+1	4.578+1	1.863+1	9.502	4.818	1.961		5.100-1
	11	1.761+3	8.690+2	3.513+2	1.774+2	8.976+1	3.653+1	1.863+1	9.446+0	3.845+0	1.961+0	

Note: M + n Implies M x 10^{+n}

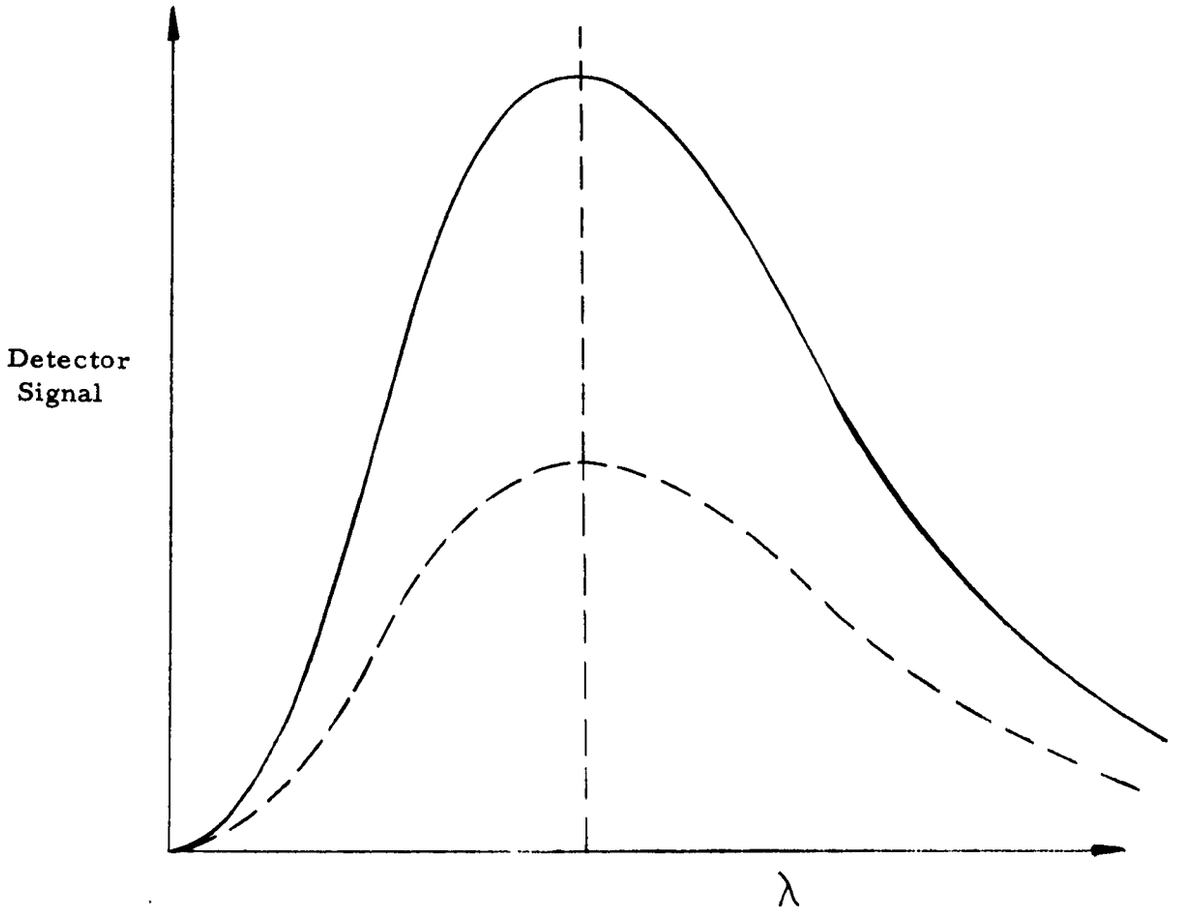

Figure B-3: Outputs of Lamps With Different Effective Source Areas But at Equal Temperatures

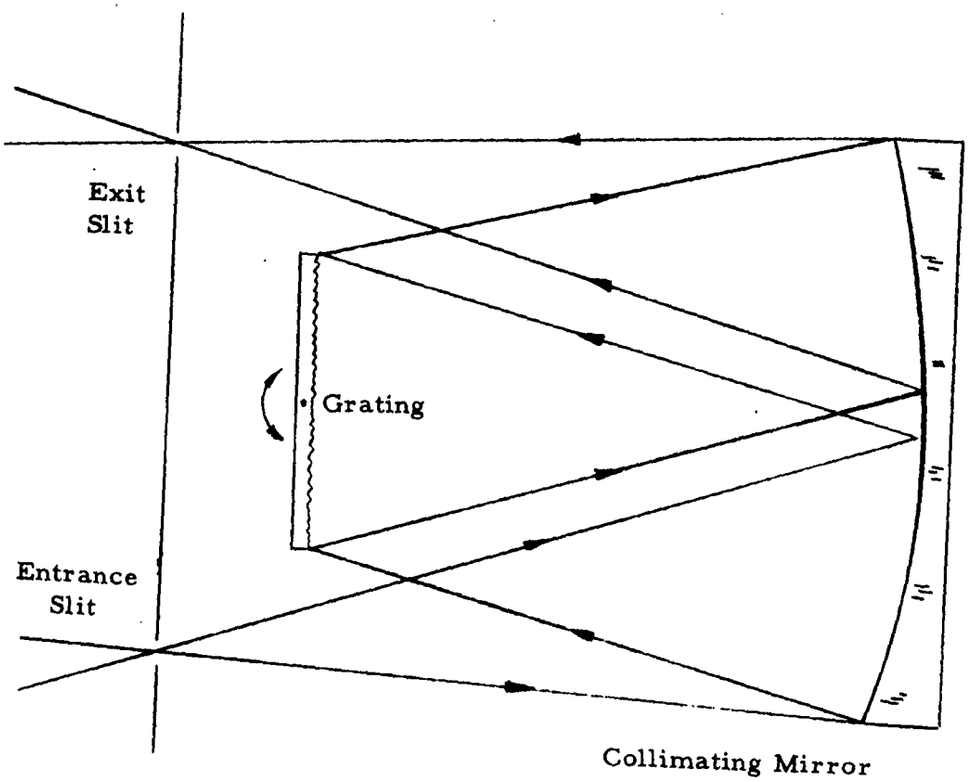

Figure B-4: Ebert Optics

Determination of Proportionality Constant

The physical units of the measurements are trivial at this stage. It is merely important that the operating and measurement conditions for the NBS lamp and the working lamp be identical. For equal temperatures, the lamp output is also a function of source area, as shown in Figure B-3. In this way, the constant of proportionality is found between the working lamp and the NBS lamp such that the spectral radiant intensity of the working lamp may be determined. In general, this proportionality will vary somewhat with the wavelength due to dissimilarities in the lamp materials. It may or may not be important to take this variation into account, depending upon the accuracy of the measurements and the extent of the variation.

II. J. A. 0.5 m. Ebert Scanning Spectrometer

The Ebert Spectrometer consists of an entrance slit, a collimating concave mirror, a blazed grating, and an exit slit (Figure B-4). For calibration, the image of the filament of the working lamp is focused upon the entrance slit and the exit slit is focused upon a photo-multiplier tube or any other detecting device. The output of the detector is amplified and used to drive a strip chart recorder. Various attenuation factors are built into the electronic recording system of the spectrometer in order to be able to uniformly distinguish spectral lines which are either very bright or very dim. These attenuation factors may be set in by turning a switch.

Intensity Calibration

In quantitative spectrographic work, it is desirable to be able to determine the radiant intensity of a given spectral line. It therefore becomes desirable to determine the response of the spectrometer to all wavelengths. This will be a function of the spectral reflectivities of the optics, spectral sensitivity of the detector, and other factors. The working lamp is placed in the position where the gas to be analyzed will be located, and the image of the filament is focused upon the entrance slit. It now remains to scan through the spectrum of the working lamp and record the photo-multiplier output. The procedure may require setting in some attenuation with the attenuation switch. Using the following table, the output is divided by the attenuation factor and then compared

with the known spectral radiance of the working lamp. Dividing each output signal by the known radiance at the given wavelength, the chart deflection per watt/steradian is determined as a function of wavelength.

Notice that the lamp must be run at the current defined by Figure B-2, and that a small error in this current will be doubled in the output. Hence it is necessary that the lamp current be monitored accurately.

Wavelength Calibration

The Ebert is calibrated for wavelength by viewing the spectrum of a standard source, such as an iron arc. The iron arc has over 300 lines in the wavelength region from 2400 Å to 6700 Å (B-1). Other standards are mercury, neon, and cesium arcs. The wavelengths are read out directly by a Veeder root counter.

It may be desirable to calibrate for wavelength before calibrating for intensity, as there may be effects (e.g., absorption lines) which influence intensity measurements at certain discrete wavelengths.

III. J. A. 1.5 m. Wadsworth Spectrograph

The Wadsworth spectrograph (see Figure B-5) consists of an entrance slit, a concave collimating mirror, a concave blazed grating, and a curved strip of film. Calibration of the device is complicated by the non-linearity of the wavelength dispersion scale and the non-linear characteristics of the photographic emulsion.

Wavelength Calibration

Fixed to the film guide is a wavelength reference marker. This shields part of the film, leaving an unexposed reference mark on the developed strip (Figure B-6). Wavelength calibration is accomplished by photographing the spectrum of a standard source, as with the Ebert spectrometer. The intensity variation is determined using a micro-densitometer, and the wavelength calibration data is recorded as λ versus micro-densitometer travel from the reference mark.

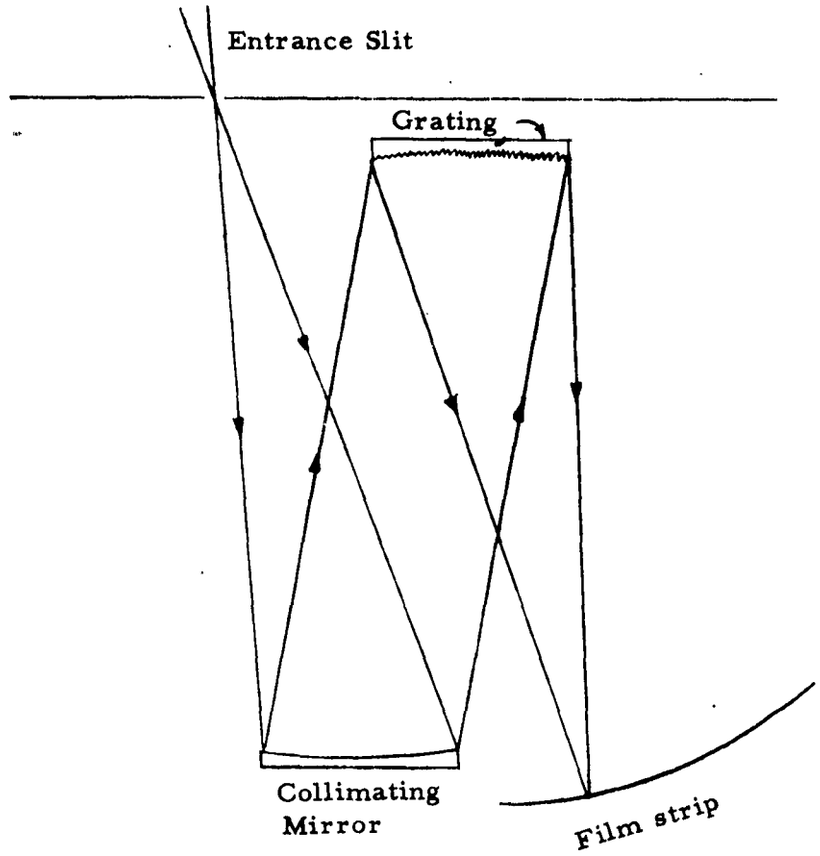

Figure B-5: Wadsworth Optics

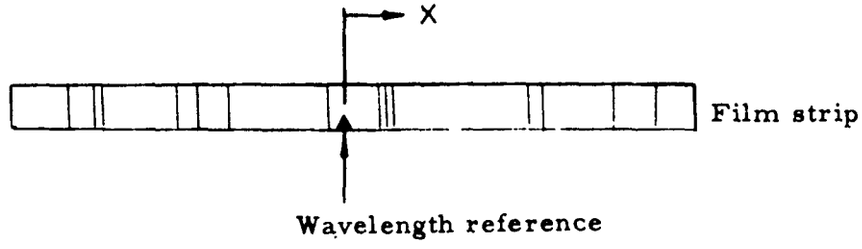

Figure B-6: Wavelength Marker

Intensity Calibration

Before it is possible to discuss the intensity calibration of the instrument, it is necessary to mention some of the characteristics of photographic emulsions [B-1] since these are used for recording the spectral data.

The photographic emulsion does not respond in a linear fashion. If one plots the density ($\log_{10} I_o/I$) versus the $\log_{10}$ of the exposure (intensity x time), a characteristic curve is obtained such as that shown in Figure B-7. For the linear portion of the curve, the density may be given as a function of the exposure raised to the γ power. All photographic emulsions exhibit dependence upon the wavelengths with which they are illuminated. Most have a variation in γ with λ for a given photographic process (Figure B-8a). All of them have a strong dependency with regard to sensitivity as a function of λ (Figure B-8b). In any case, the selection of an emulsion depends upon the wavelength region to be investigated, and it may be necessary to use several emulsions to cover the desired wavelength range. Thus, the selection of suitable photographic emulsion is the first step in the intensity calibration procedure. By careful selection of a development procedure, it is possible to make γ equal to one, in which case the density is directly proportional to the exposure. Once the development process has been fixed, one finds it desirable to operate in the range of exposures in which the characteristic curve is linear. Thus, the determination of a standard development technique for the chosen emulsion is the second step in the intensity calibration procedure.

A final consideration in the discussion of emulsions is the reciprocity law of Bunsen and Roscoe, which states that the exposure is equal to the product of the intensity and the exposure time. It has been shown that equal exposures do not produce equal effects on the film (reciprocity-law failure). Furthermore, when (as with the Wadsworth) the exposure along the slit is varied by spinning a stepped sector over the entrance slit (Figure B-9), the intermittent exposures do not produce the same effect as equivalent continuous exposures except above a critical frequency (intermittency effect). For most films a safe operating frequency is about 1600 rpm, although with some emulsions (and this is important) there is always an intermittency effect with the sector arrangement [B-1]. It is important that the illumination is constant over the slit.

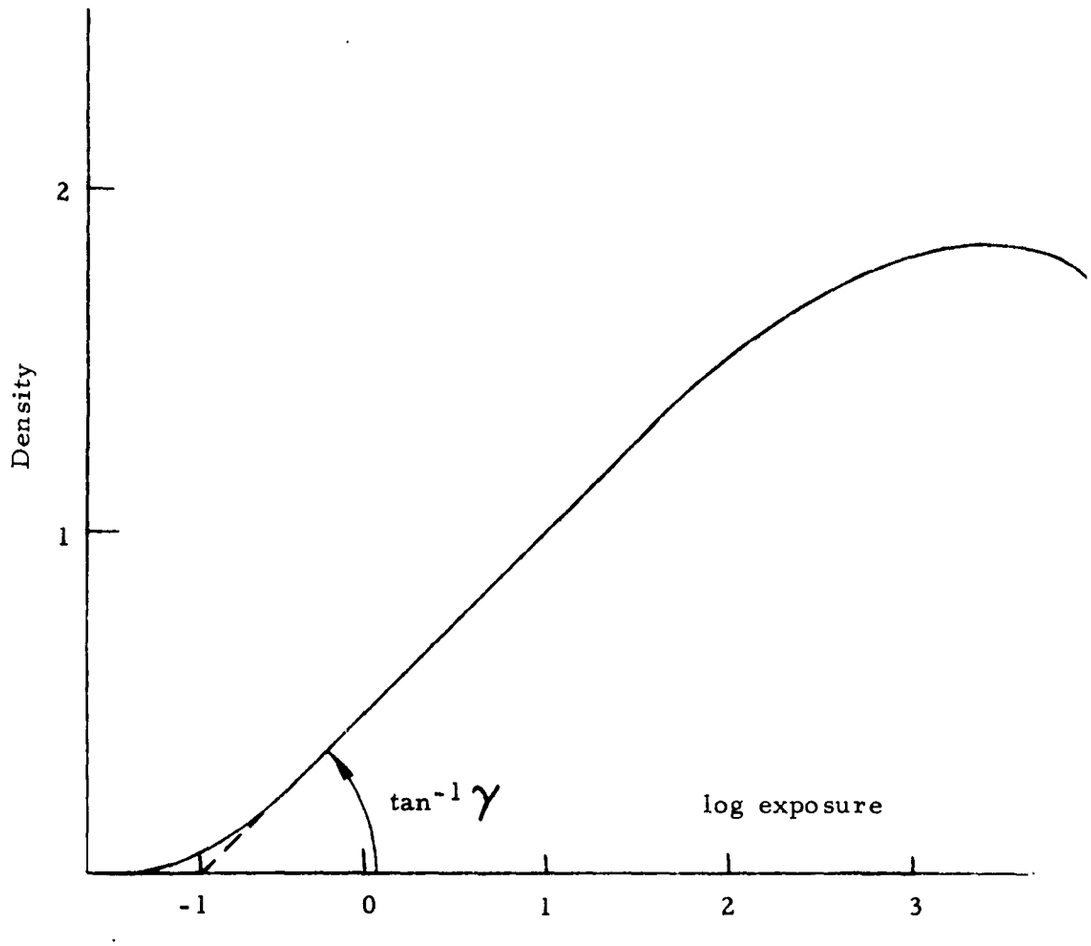

Figure B-7: Characteristic Curve

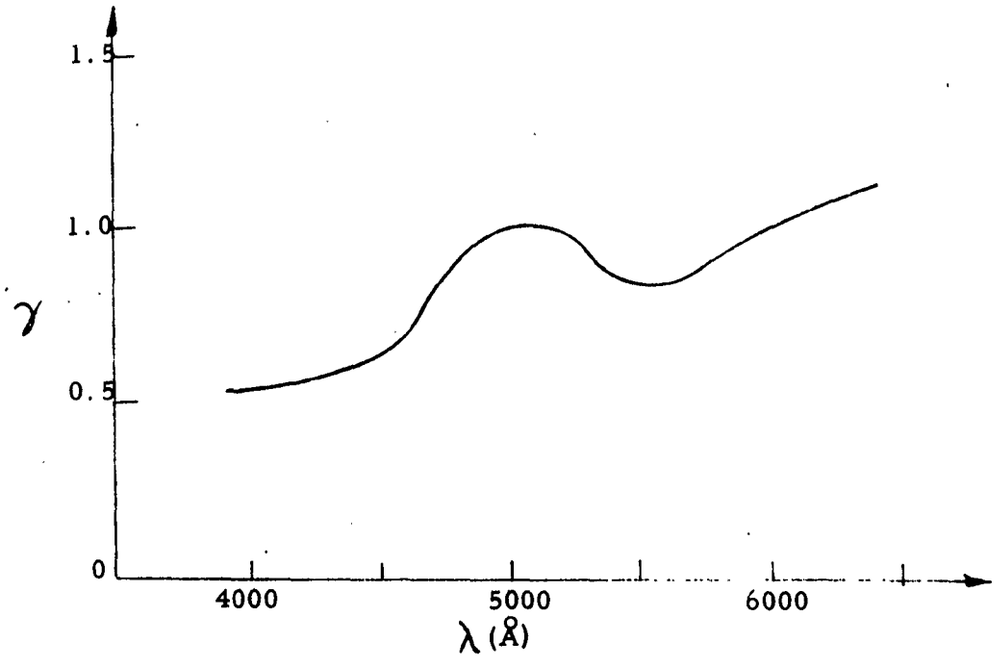

B - 8 (a)

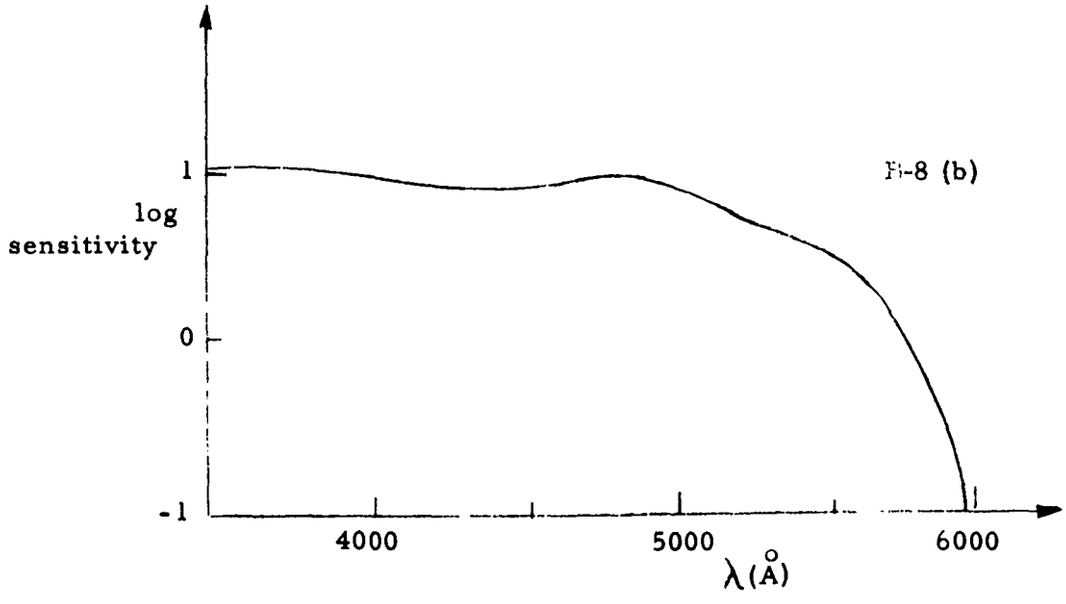

Fi-8 (b)

Figure B-8: Emulsion Characteristics

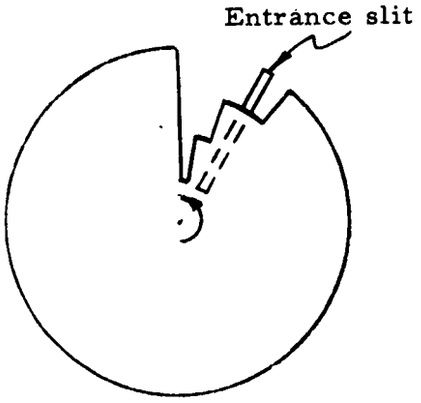

Figure B-9: Stepped Sector

Hence, the ribbon filament is especially desirable in calibration work since it gives relatively uniform illumination over the entire entrance slit.

Once an emulsion is chosen, it is placed in the spectrograph and the working lamp spectrum is photographed. Micro-densitometer traces are made of the resulting negatives, and a similar procedure is followed to determine the wavelength response as for the Ebert spectrometer. It is important here to try several exposure conditions to determine if one is operating in the linear region of the film.

REFERENCES

B-1 Sawyer, R.A.; Experimental Spectroscopy; Prentice-Hall; New York, 1946.

APPENDIX C

MEASUREMENT OF ION DENSITIES USING THE HOLTZMARK THEORY OF LINE BROADENING

Theory

It is shown by Holtzmark [C-1] that the average electric field at a radiating atom in a plasma due to the ions alone is (for singly charged ions):

$$E_o = 2.61\, e\, n_i^{2/3} \qquad \text{(C-1)}$$

where e = electronic charge and n_i = ion density. The statistical distribution of the electric field (isotropic) is also shown to be

$$W(\beta)\, d\beta = 1.496\beta^{-5/2}\,(1 + 5.106\beta^{-3/2} + 14.43\beta^{-3} + \ldots)\, d\beta \qquad \text{(C-2)}$$

$$\simeq \frac{3}{2}\beta^{-5/2}\, d\beta \quad [\beta \text{ large}] \qquad \text{(C-2a)}$$

$$\text{where } \beta \equiv \frac{E}{E_o} = \left(\frac{r_o}{r}\right)^2 \qquad \text{(C-3)}$$

and r is the distance between the ion and radiator.

Note that β large imples small γ (i.e., close encounters) and the latter form (C-2a) applies for the large E (i.e., in the wings of the spectral line).

The first order Stark effect gives the displacement of the perturbed line from the original undisturbed line center as being proportional to the electric field strength:

$$\Delta \nu = C_k E \qquad \text{(C-4)}$$

where $\Delta\lambda$ is the line shift (in angstroms) and C_k is the proportionality constant for the particular component. Thus

$$\beta = \frac{\Delta\lambda}{C_k\ E_o} \tag{C-5}$$

If the unperturbed spectral line consists of several components whose intensity and Stark coefficients differ, then the observed line will consist of the sum of terms

$$J\left(\frac{\Delta\lambda}{E_o}\right)\ d\left(\frac{\Delta\lambda}{E_o}\right) = \sum_k A_k\ W\left(\frac{\Delta\lambda}{C_k\ E_o}\right)\ d\left(\frac{\Delta\lambda}{C_k\ E_o}\right) \tag{C-6}$$

where $J\left(\frac{\Delta\lambda}{E_o}\right) d\left(\frac{\Delta\lambda}{E_o}\right)$ represents the line intensity in the interval $d(\Delta\lambda)$ about $\Delta\lambda$ and A_k is the transition probability of the k^{th} component of the line in question.

Equation (C-6) may be written in terms of the parameter $\alpha \equiv \frac{\Delta\lambda}{E_o}$

$$J(\alpha)\ d\alpha = \sum_k \frac{A_k}{C_k}\ W\left(\frac{\alpha}{C_k}\right)\ d\alpha \tag{C-7}$$

$J(\alpha)$ is readily computed using the known values of A_k, C_k, and Equation (C-2).

The parameter α has been defined as:

$$\alpha \equiv \frac{\Delta\lambda}{E_o} \text{ in } \mathring{A} \text{ kilovolt} \tag{C-8}$$

where $\Delta\lambda$ is the displacement from the line center and E_o is the normalized electric field strength which is related to the electron density by:

$$n_i = \left[\frac{E_o}{2.61\ e}\right]^{3/2} \tag{C-9}$$

where e = electronic charge = 4.8025×10^{-10} esu

E_o = normalized electric field

= esu volts = 300 volts

= 0.3 kilovolts

from the definition of α it is seen that $\frac{\Delta\lambda_1 - \Delta\lambda_2}{\Delta\lambda_1} = \frac{\alpha_1 - \alpha_2}{\alpha_1} = C$ (C-10)

The theoretical profiles have been replotted in Figures C-1, C-2, and C-3 to give

$$I_{R_{theo}} = \frac{I_{R_{\alpha_1}}}{I_{R_{\alpha_2}}} \text{ vs. } \alpha_1 \text{ for } C = 0.5$$

If one plots

$$I_{R_{exp}} = \frac{I_{R_{\Delta\lambda_1}}}{I_{R_{\Delta\lambda_2}}} = \frac{I_{R_{\alpha_1}}}{I_{R_{\alpha_2}}} \qquad \text{(C-11)}$$

vs. $\Delta\lambda_1$ for $\frac{\Delta\lambda_1 - \Delta\lambda_2}{\Delta\lambda_1} = C = 0.5$, as in Figures C-4 and C-5, the proper value of α_1 and $\Delta\lambda_1$ is obtained immediately from the second equality in (C-11).

Application of (C-1) and (C-2) yields the required electron concentration.

Because of the limitations of the theory, the method is not applicable near the center of the line and no attempt should be made to fit the center. A little experience will give the necessary feel for the best fit.

Because of the difficulty of reading the experimental data, Figure C-6, at the wings of the line, the profile may be plotted on log-log paper and extrapolated with a straight line. The slope will usually be found to be -5/2 as in Figure C-7 and the required data read off.

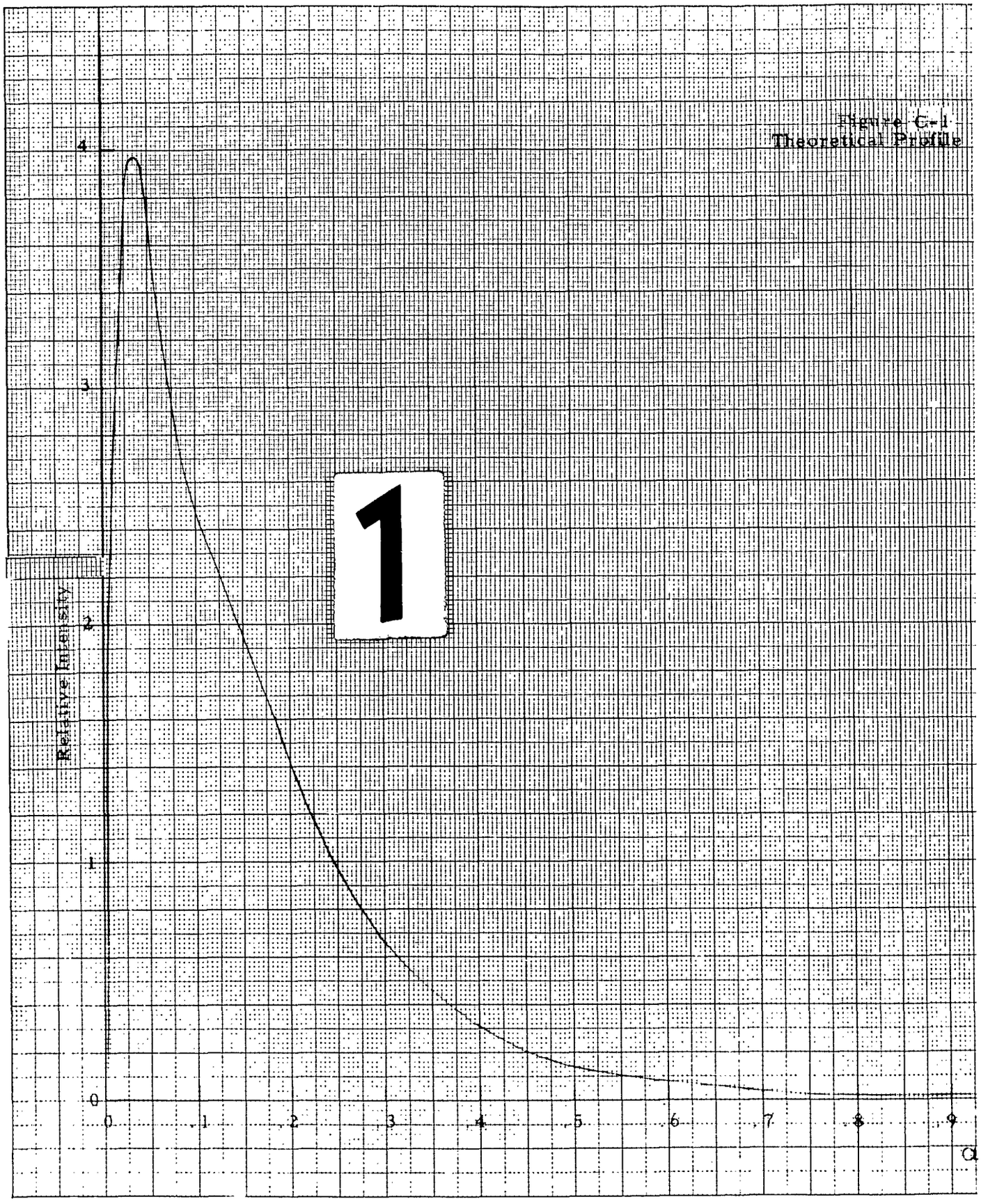

Figure C-1
Theoretical Profile

Figure C-1
Theoretical Profile H_α

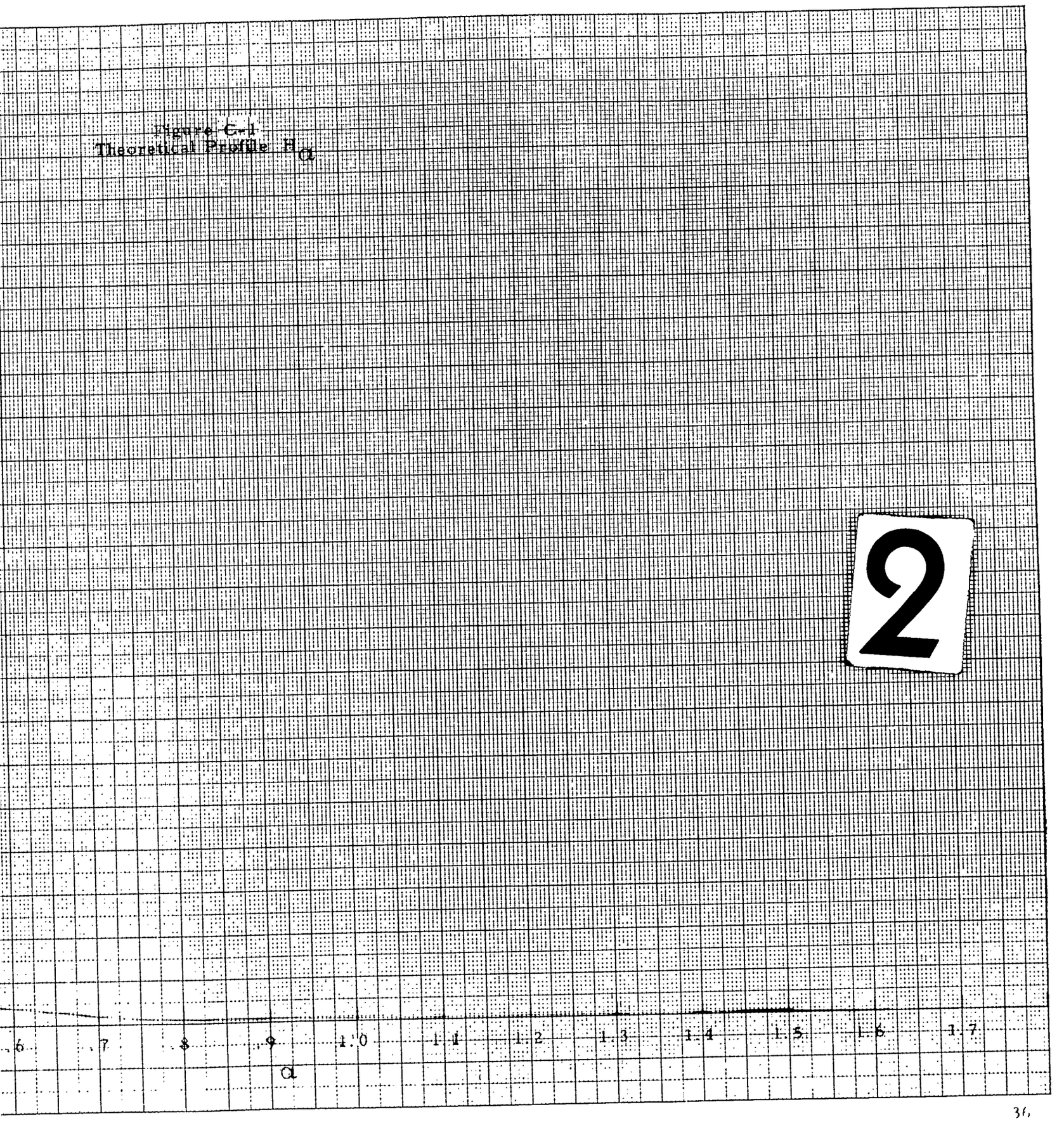

Figure C-2
Theoretical H_β Profile

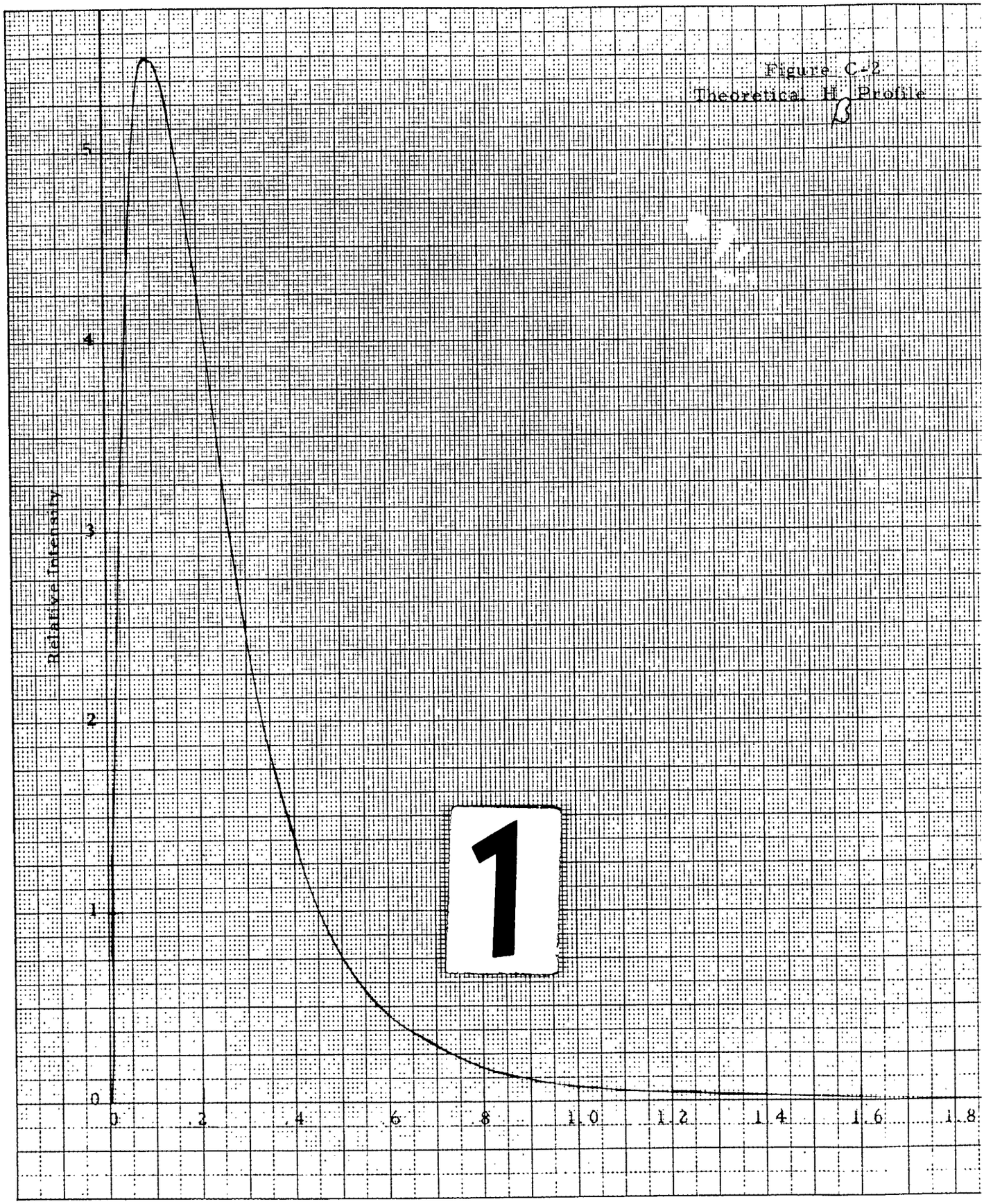

Figure C-2
Theoretical H_β Profile

1.2 1.4 1.6 1.8 2.0 2.2 2.4 2.6

α

Figure C-3

Theoretical Profile H_Y

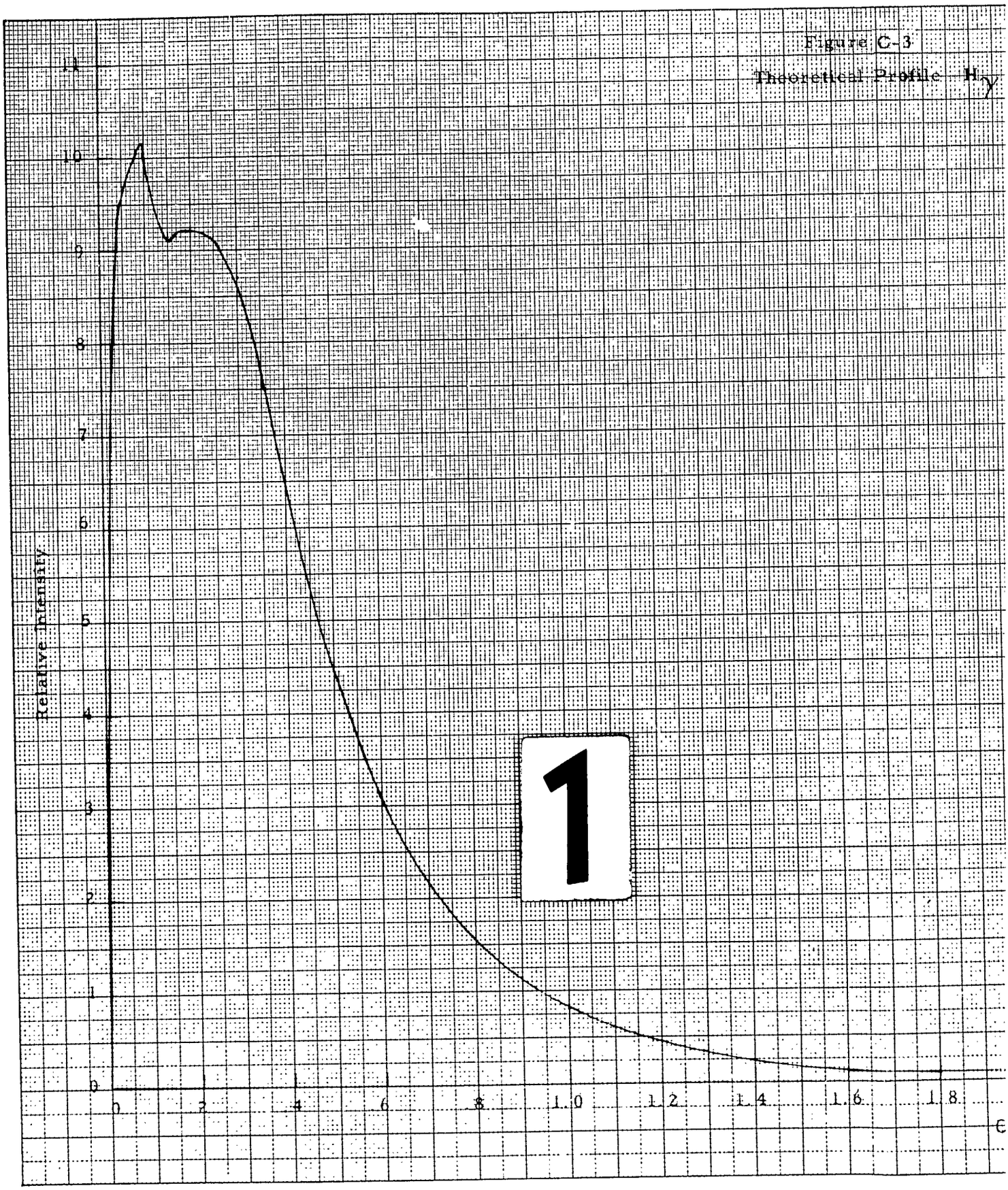

Figure C-3

Theoretical Profile H_y

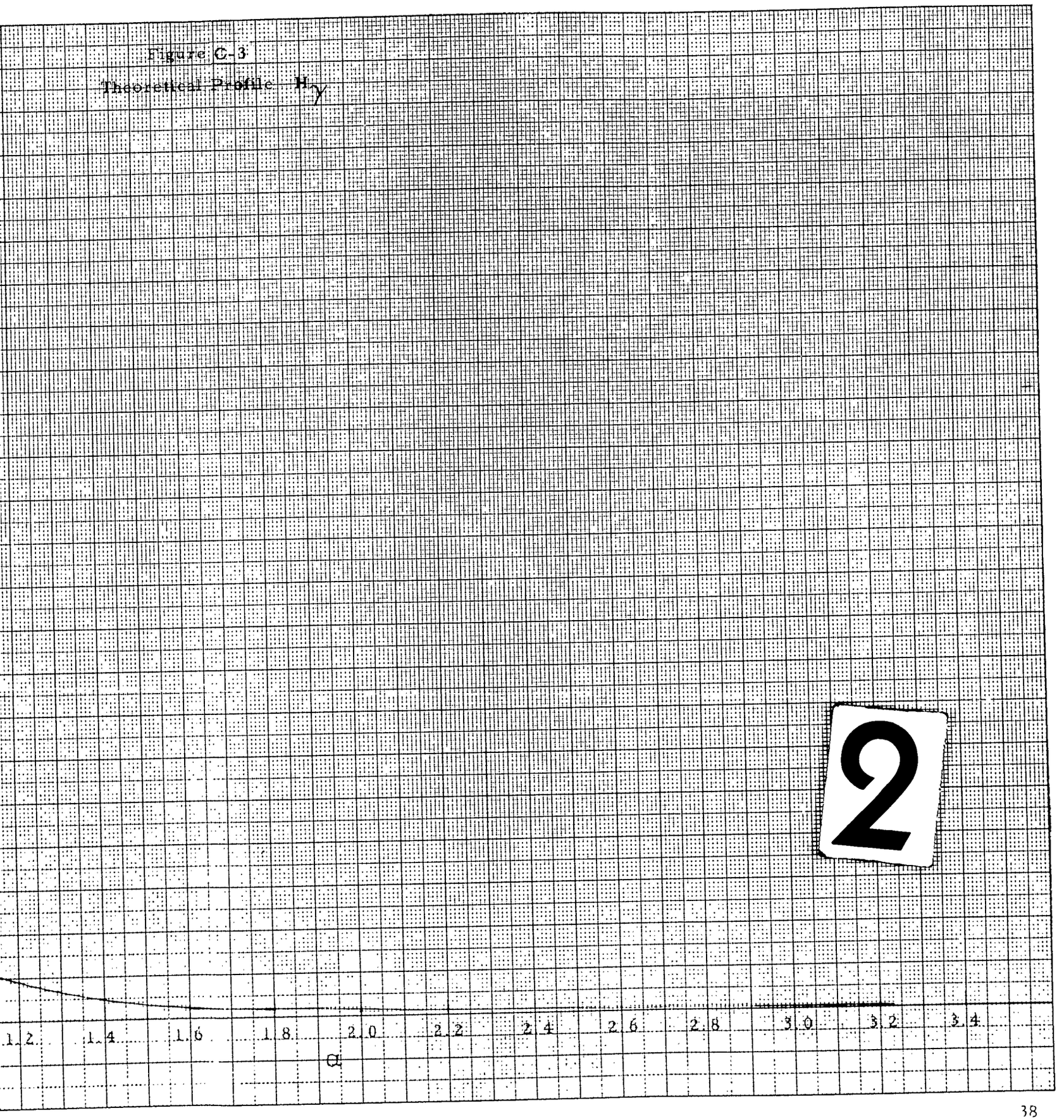

K+E 10 X 10 TO THE C.M. 359-14
KEUFFEL & ESSER CO MADE IN U.S.A.

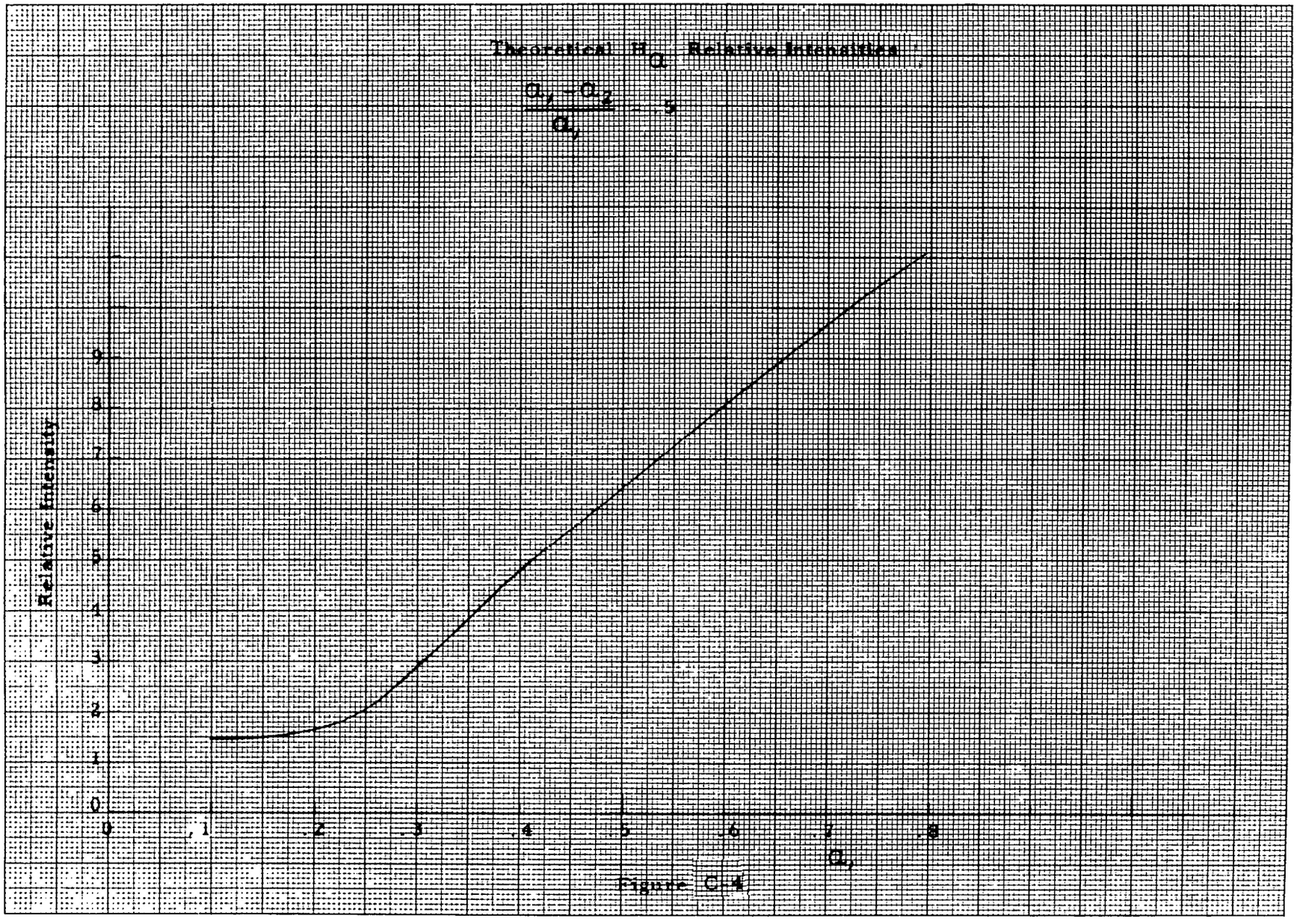

Figure C-4

K&E 10 T CM 3-14
KEUFFEL & ESSER CO.

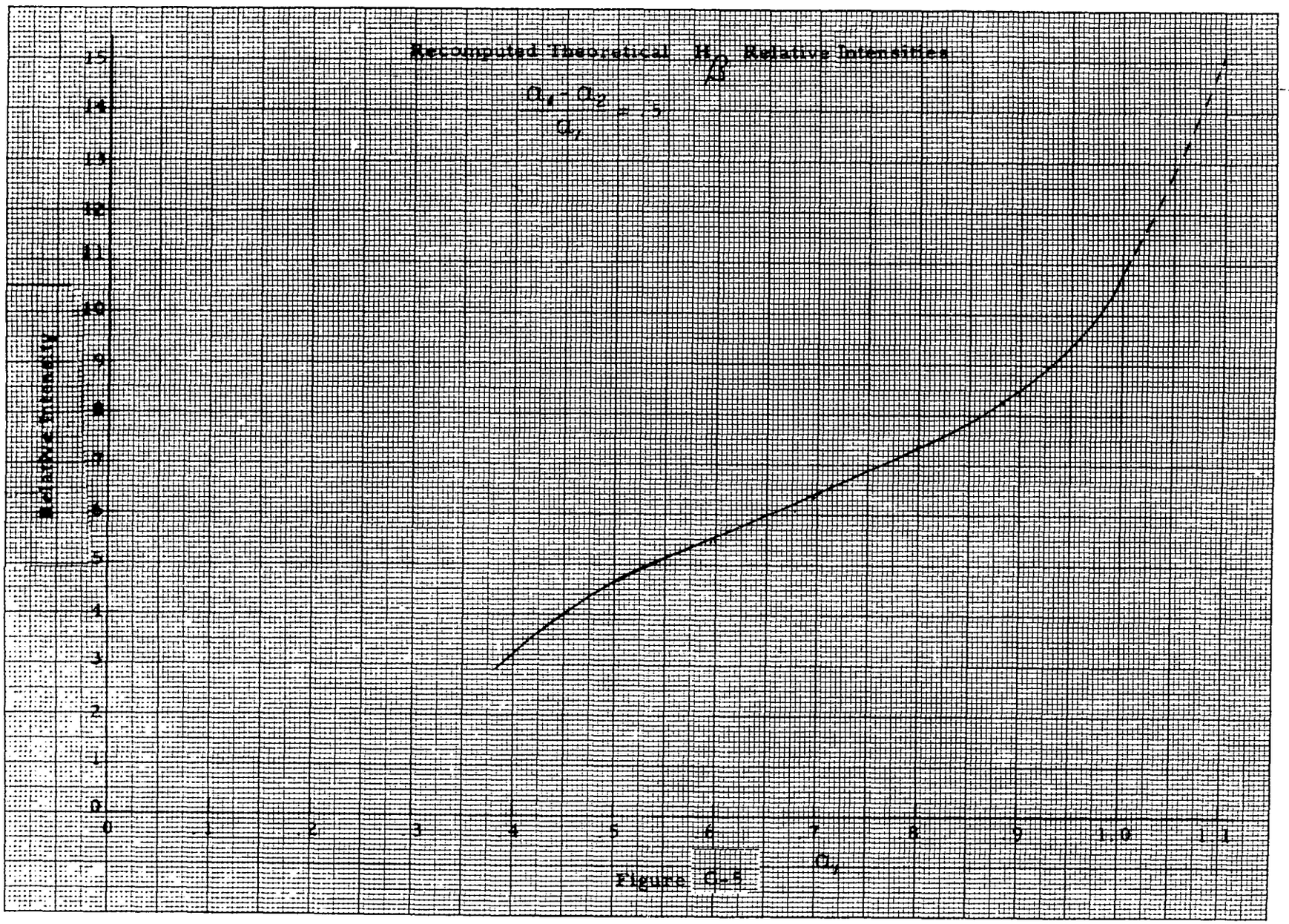

Figure C-5

K&E 10 X 10 TO THE CM. 359-1
KEUFFEL & ESSER CO. MADE IN U.S.A.

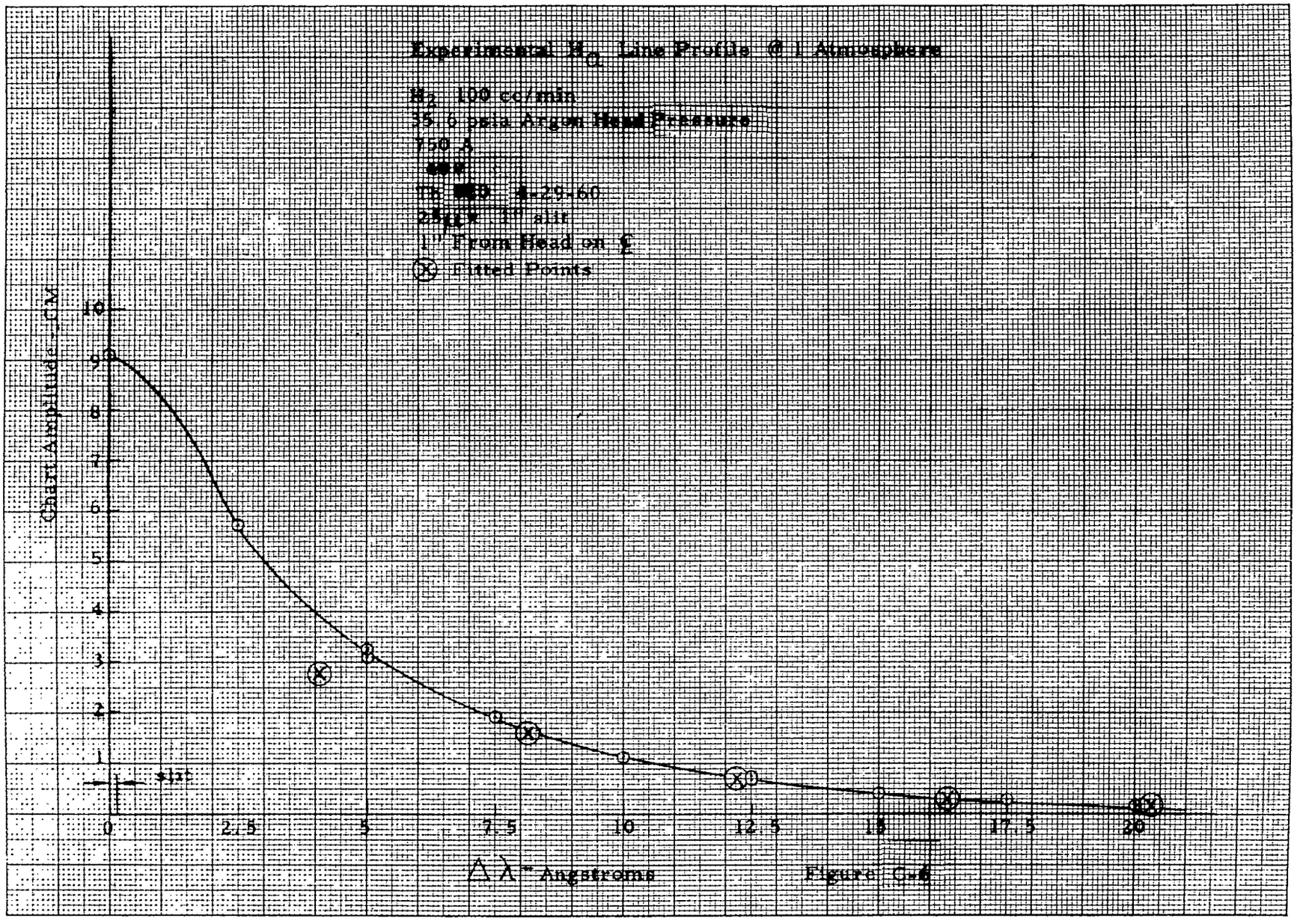

Figure C-6

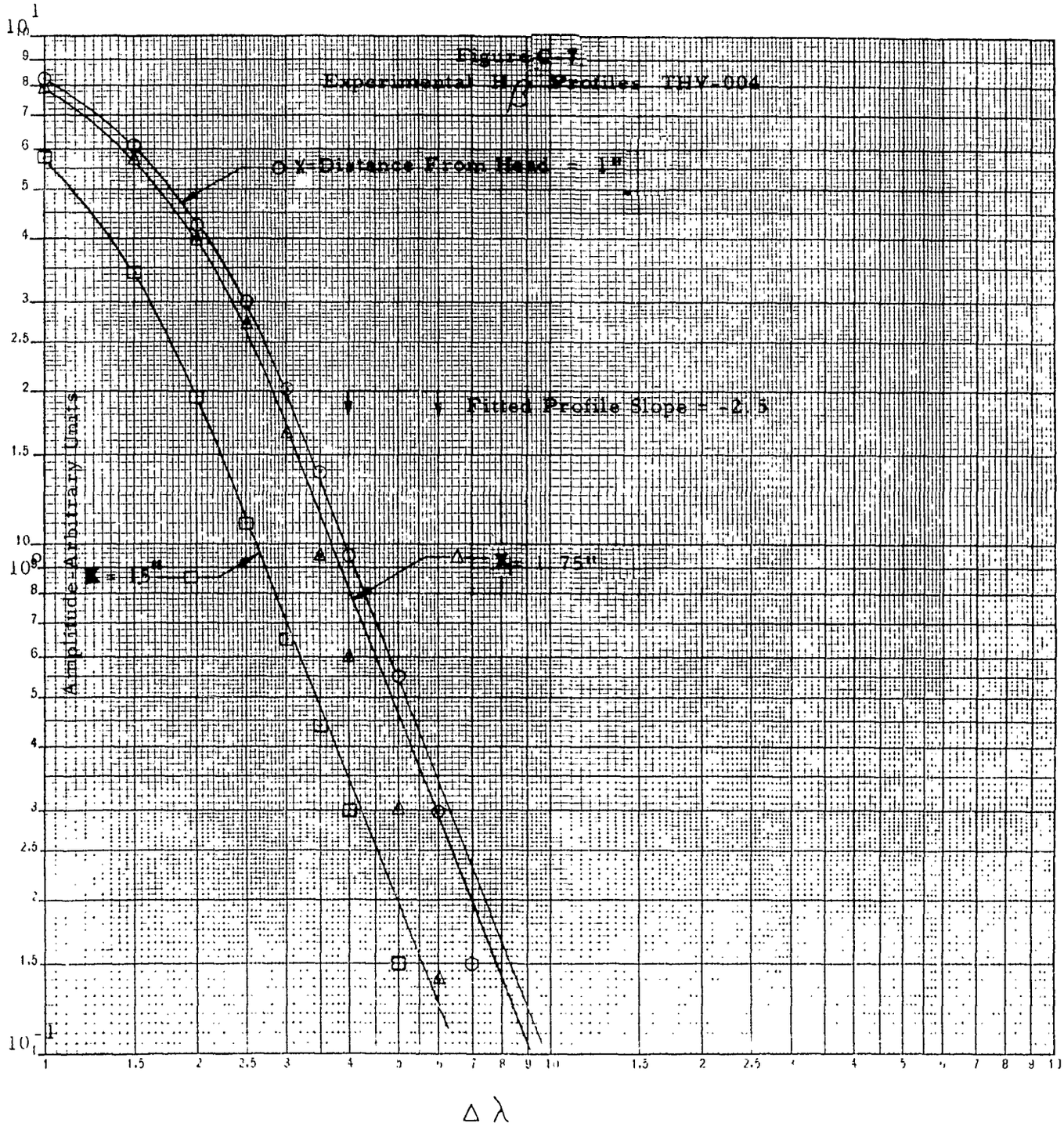
Figure C-7
Experimental H_β Profiles THV-004
X-Distance From Head = 1"
Fitted Profile Slope = -2.5
Amplitude-Arbitrary Units
Δλ

For this analysis the experimental data need not be corrected for phototube response since the response will not vary appreciably within the wavelength span of a single line and only relative values of amplitudes are required. In practice, the result from a single line should not be considered conclusive. Comparison with the results of other lines should be made. In general the results may differ by a factor of 2 or so. The final result depends upon the quality of the data and the theoretical fit.

Note that while the theory apparently indicates a shift in one direction only, the quantum mechanics of the Stark effect shows a symmetrical splitting, and for linear Stark effect the center of the line is not displaced. If desired, both sides of the measured line may be used for analysis and the results averaged since it is sometimes difficult to read the precise center from the data. Occasionally, for broad lines, the background or other close lines will dictate the most convenient half of the line to be used.

References

C-1 Holtzmark, J.; Physic Z. 20, 162 (1919).

APPENDIX D

ALTERNATE METHOD OF ION DENSITY MEASUREMENT

The results of a more rigorous derivation of the broadening effect of ions and electrons is given by Griem [D-1] in which the half width at half height of several lines in the visible cesium spectrum are shown as a linear function of electron density with a slight dependence on temperature. The theoretical details for Griem's calculations are not available and hence the form of the temperature dependence is not known. In view of the small variations and other uncertainties it will be assumed that linear interpolation is sufficient. This should certainly lead to errors no larger than the rough estimate of 10% to 20% of the ion broadening effect.

The numerical data is given in Appendix J.

The data reduction procedure is extremely simple:

1. Determine the temperature by the methods of Appendix E.
2. Measure the half width at half height for the prominent Cs lines. (See Figure D-1)
3. Interpolate between tabulated values to obtain theoretical broadening at the measured temperature.
4. Scale the electron density directly with line width with a 0.8 to 0.9 reduction due to the ion broadening effect.

If $(\frac{\omega}{2})^{\circ}_{2500}$ and $(\frac{\omega}{2})^{\circ}_{5000}$ are the theoretical broadening values at the reference electron density (10^{16}/cc) and temperature, then

$$\left(\frac{\omega}{2}\right)^{\circ}_{T} = \left(\frac{\omega}{2}\right)^{\circ}_{2500} + \left[\left(\frac{\omega}{2}\right)^{\circ}_{5000} - \left(\frac{\omega}{2}\right)^{\circ}_{2500}\right]\left(\frac{T-2500}{2500}\right)$$

is the reference broadening at the measured temperature T ($^{\circ}$K).

The measured electron density is then:

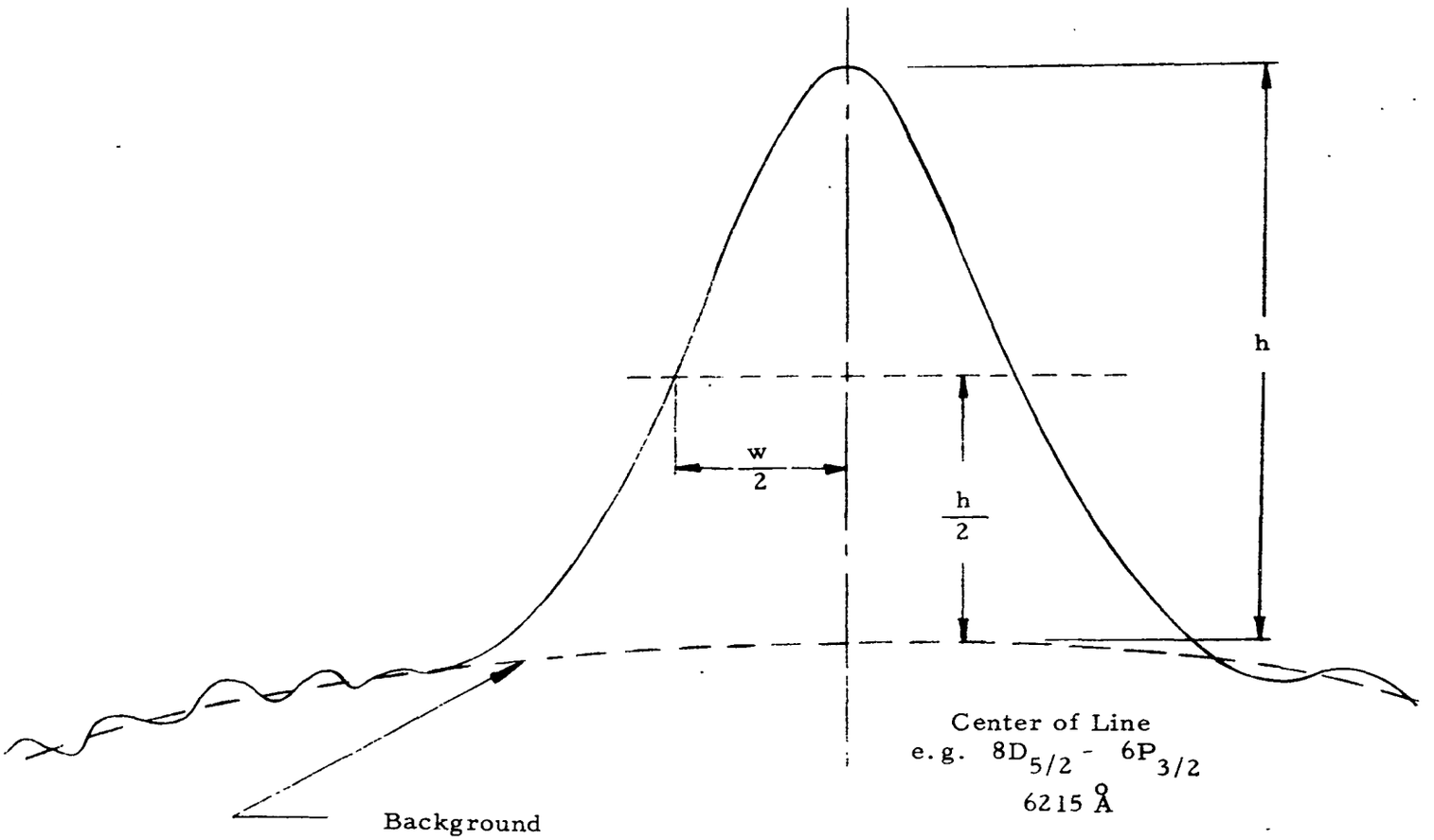

Figure D-1: Schematic of a Spectral Line

$$\frac{\phi \left(\frac{\omega}{2}\right)_{meas}}{\left(\frac{\omega}{2}\right)_{T}^{o}} \times 10^{16} = e/cc$$

where ϕ is a parameter accounting for the ion broadening and is typically 0.8 to 0.9.

References

D-1 Griem, H., Personal Communication

APPENDIX E

OPTICAL METHODS OF TEMPERATURE DETERMINATION

Temperature profiles must be determined in two specific regions: in all phases of the program, gas temperature levels are required; in the ablation experiment, the surface temperature of the test model must also be obtained.

Black Body Radiation

The radiation from the surface of the ablation test model is considered to be characteristic of a black body at the surface temperature of the model. Thus, the intensity is given by:

$$I_\lambda = K \frac{c_1}{\lambda^5} \left[\exp\left(\frac{c_2}{\lambda T}\right) - 1\right]^{-1} \qquad \text{(E-1)}$$

where I is the radiant intensity in units of power per unit area,

K is constant depending on the optics of the system and the emissivity of the body under analysis, c_1, c_2 are the first and second radiation constants, respectively, λ is the specific wavelength at which the intensity measurement is made, and T is the temperature of the radiating surface.

Consideration of the a priori limits imposed on the experiment allows a further simplification of Equation (E-1). Thus, the surface temperature of the test model can be expected not to exceed 4000°K (melting point of graphite 3900°K), and the response of the phototube in the optical system limits the useable wavelength region to 4000 Å to 9000 Å, nominally. Substitution of these maximum values (i.e. $\lambda T \leq$ 36 cm°K) into Equation (E-1) shows that, to within 2%.

$$I_\lambda = K \frac{c_1}{\lambda^5} \exp\left(-\frac{c_2}{\lambda T}\right) \qquad \text{(E-1a)}$$

The evaluation of local surface temperature proceeds from the relative intensities, measured at two different wavelengths, radiating from the same element of body surface area. The ratio of two intensity measurements is given by:

$$\frac{I_{\lambda 1}}{I_{\lambda 2}} = \left(\frac{\lambda_2}{\lambda_1}\right)^5 \exp\left(\frac{c_2}{\lambda_2 T} - \frac{c_2}{\lambda_1 T}\right) \qquad \text{(E-2)}$$

The temperature is then given by:

$$T = c_2 \left[\frac{\lambda_1 - \lambda_2}{\lambda_1 \lambda_2}\right] \left[\ln\left(\frac{I_{\lambda 1}}{I_{\lambda 2}}\right) + 5 \ln\left(\frac{\lambda_1}{\lambda_2}\right)\right]^{-1}$$

It is seen from Equation (E-3) that, as λ_2 approaches λ_1, T becomes the ratio of two numbers close to zero. Thus, to ensure better accuracy, the comparison of measured intensities should be carried out for wavelengths as far apart as possible. Also, the ratios of several measurements should be used, and a mean value of the computed temperature determined.

The value of c_2 required is dependent on the units used for λ. For λ in Angstrom units,

$$c_2 = \frac{hc}{k} = 1.4387 \times 10^8 \ \text{Å} - {}^{\circ}\text{K}$$

The expected error in a single temperature value cannot be estimated a priori, due to the complicated dependence of T on both the measured intensity and the wavelength at which the intensity measurement is made. Differentiating Equation (E-3), a formula for the relative error in T, as a function of the uncertainty in the measured intensity is:

$$\frac{\Delta T}{T} = - \left[\ln\left(\frac{I_{\lambda 1}}{I_{\lambda 2}}\right) + 5 \ln\left(\frac{\lambda_1}{\lambda_2}\right)\right]^{-1} \left[\frac{\Delta I_1}{I_1} - \frac{\Delta I_2}{I_2}\right] \qquad \text{(E-4)}$$

Thus, the experimental data will allow an estimation of the theoretical error.

Gas Phase - Line Spectra

The spectral radiation from several gas constituents will be used to determine the temperature of the flow both around the ablation test model and from $CsNO_3$: Al rocket motor. The emitting species in the rocket motor exhaust will be cesium and aluminum. In the ablation tests, sodium and potassium will be used as well. In addition, it may be necessary to seed

the argon of the plasma jet with hydrogen in order to obtain emission in the proper spectral region. The theoretical basis for data reduction, as well as the requisite data for the radiating species, are given below.

The measured intensity of a spectral line is given by:

$$I_i = KA_i \frac{hc}{\lambda_i} N_i \qquad \text{(E-5)}$$

where K is a constant of the optical system,

A_i is the transition probability of the transition under consideration,

h is Planck's constant,

c is the speed of light in vacuo,

λ_i is the wavelength of emitted radiation, and

N_i is the number density of particles of the radiating specie in the upper state of the transition in question.

N_i is assumed to obey the Maxwell-Boltzmann distribution law, i.e.

$$N_i = N \frac{g_i e^{-E_i/kT}}{\sum_j g_j e^{-E_j/kT}} \qquad \text{(E-6)}$$

$$= \frac{N}{Q} g_i e^{-E_i/kT}$$

where N is the total number density of the radiating specie,

g_i is the degeneracy of the upper state of the transition,

E_i is the energy of this upper state,

k is the Boltzmann constant,

T is the local temperature, and

Q, as defined in Equation 6, is the partition function of the radiating specie.

By direct substitution of Equation (E-6) into Equation (E-5), we have

$$I = KA \frac{hc}{\lambda} \frac{N}{Q} ge^{-E/kT} \qquad \text{(E-7)}$$

or

$$\ln\left(\frac{I\lambda}{Ag}\right) = \ln\left(K\, hc \frac{N}{Q}\right) - \frac{E}{k} \frac{1}{T} \qquad \text{(E-7a)}$$

Thus, it is seen that if we plot $\ln(\frac{I\lambda}{Ag})$ versus (E/k) (i.e., the energy level expressed as an equivalent temperature) the magnitude of the slope of the resulting straight line plot will be the reciprocal of the desired temperature value, algebraically:

$$T = - \frac{1}{\frac{d}{d(E/k)} \left(\ln \frac{I\lambda}{Ag}\right)} \qquad \text{(E-8)}$$

The slope of the line may be approximately determined by an empirical "best fit" or by a least squares fit on a computer. A check on the results may be obtained by using a relative intensity method similar to that described for the black-body data reduction.

The relative error in the temperature due to experimental uncertainty in the intensity values may be obtained from Equation (E-7) by differentation. Thus

$$I = KA \frac{hc}{\lambda} \frac{N}{Q} ge^{-E/kT} \qquad \text{(E-7)}$$

$$\Delta I = KA \frac{hc}{\lambda} \frac{N}{Q} g \left[\frac{E \Delta T}{kT^2}\right] e^{-E/kT} \qquad \text{(E-7b)}$$

and

$$\frac{\Delta I}{I} = \frac{E}{kT} \quad \frac{\Delta T}{T} \tag{E-9}$$

or

$$\frac{\Delta T}{T} = \frac{kT}{E} \quad \frac{\Delta I}{I} \tag{E-9a}$$

Therefore, the variation in T may be determined from the experimental data for each specific line.

The various constants required in the above equations are presented in Appendix J.

APPENDIX F

DETERMINATION OF RADIATING SPECIE CONCENTRATIONS BY A NUMERICAL SOLUTION OF ABEL'S INTEGRAL EQUATION

The method outlined below was presented by Pearce [F-1]. The data to be reduced will be in the form of photographic plates from which relative radiant intensity may be determined.

It is assumed that the plasma is cylindrically symmetric, and that the concentration of radiating species varies as a radial step-function. (See Figure F-1). The photographic raw data is then divided into an arbitrary number of equally spaced segments on this basis.

The analysis begins with the last segment of the photographic data. The intensity, I_n, is known and we wish to find the radiating specie concentration. Thus, from the figure,

$$I_n = \Delta A_{n,n} \quad N_n$$

$\Delta A_{n,n}$ is found in the referenced work in tabular form for n less than or equal to 25.

Proceeding,

$$I_{n-1} = N_n (\Delta A_{n-1,n}) + N_{n-1} (\Delta A_{n-1,n-1})$$

where the unknown is now N_{n-1}.

In general, N_j is found from

$$I_j = \sum_{k=j}^{n} N_K \Delta A_{j,k} \qquad (j = n, n-1, \ldots 2, 1)$$

The analysis thus produces one annular concentration value at a time, beginning at the outside of the plasma, and working into the central core.

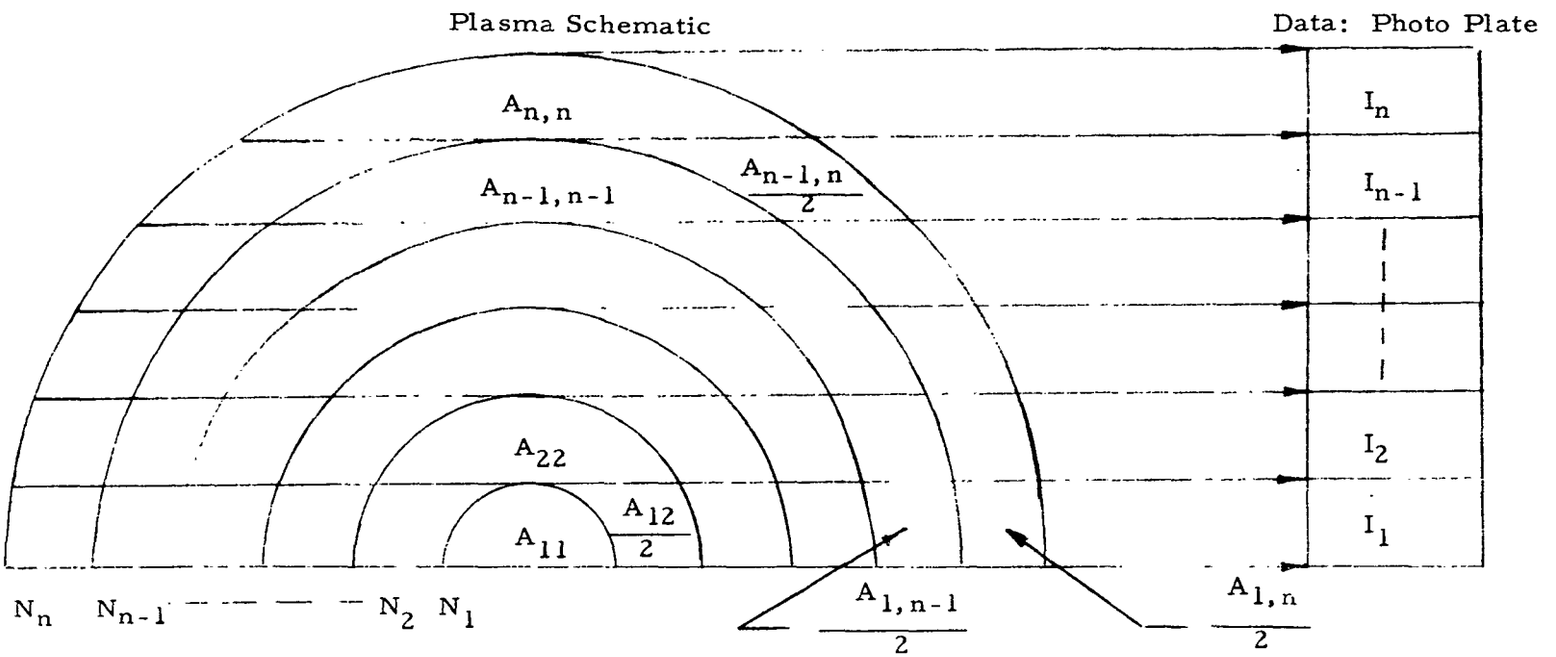

Figure F-1: Concentration Determination

References

F-1 Pearce, W. J.; "Calculation of the Radial Distribution of Photon Emitters in Symmetric Sources"; Conference on Extremely High Temperatures; Wiley; New York; 1958.

APPENDIX G

BOUNDARY LAYER VELOCITY PROFILE

It is the purpose of this appendix to describe an approximate method for deducing the boundary layer velocity profile from corresponding thermal boundary layer data. The latter is to be obtained from plasma-jet tests of either blunted or conically tipped cylinders using argon gas as the basic working medium.

It is anticipated that the plasma-jet test facility will be such that the argon gas will be chemically frozen after expansion from its initial reservoir (stagnation) conditions prior to flow about the test body. As a result, the associated aerodynamic flow processes are assumed to be calorically perfect.

The final choice of the body shape will most likely be dictated by the existing condition of the test model material, namely right cylindrical shapes of high slenderness ratios. Although such bodies are difficult to analyze, little would be gained from the use of other shapes due to lack of simple analytical solutions (or experimental data corresponding to anticipated conditions) to their associated flow fields. Further, if the region under examination lies several body diameters downstream of the frontal nose-cylinder junction then the inviscid flow will approximate free stream conditions regardless of the nose shape. Because of its inherent simplicity, such an arrangement will be assumed.

Normally, simple solutions to the viscous boundary layer flow do not exist. However, under certain restrictive assumptions, reasonable relationships may be obtained which are directly applicable to the expressed problem. The Crocco analysis for compressible viscous flow with a Prandtl number of unity is such a case [G-1]. Without going into the details, the basic assumptions are tabulated below:

(a) No pressure gradient along the body surface

(b) No temperature gradient along the body surface

(c) Steady-state conditions

(d) Constant Prandtl number.

If the test point is located far downstream of the nose the first two assumptions will be satisfied. The validity of the third assumption depends on the length of the test and model size. The final assumption is rigorously invalid but appears to approximate actual conditions as the Prandtl number ranges from roughly 0.6 at 0°C to 1.1 at 1200°C. The analysis yields the following simple relationship between velocity and enthalpy:

$$h_B = h_W - (h_W - h_A)\frac{u}{U_E} - (h_A - h_E)\left(\frac{u}{U_E}\right)^2$$

For constant specific heats this reduces to:

$$T_B = T_W + (T_A - T_W)\left(\frac{u}{U_E}\right) - (T_A - T_E)\left(\frac{u}{U_E}\right)^2$$

Solving for $\frac{u}{U_E}$:

$$\frac{u}{U_E} = \frac{(T_A - T_W) + \sqrt{(T_A - T_W)^2 - 4(T_A - T_E)(T_B - T_W)}}{2(T_A - T_E)}$$

where

U_E = boundary layer edge velocity (in this case U_E is assumed equal to the free stream velocity)

u = local boundary layer velocity

T_E = boundary layer edge temperature

T_W = wall temperature

T_B = local boundary layer temperature

T_A = adiabatic temperature (assumed equal to reservoir temperature)

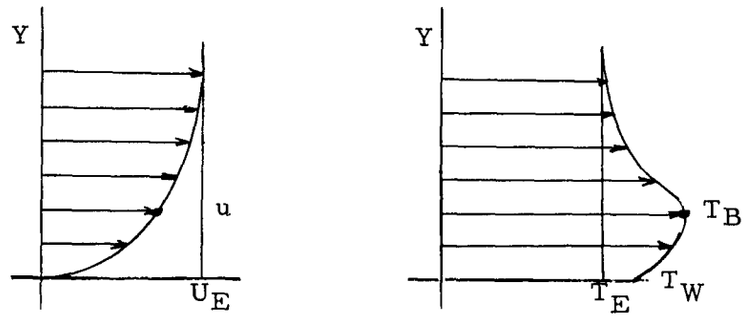

Thus from a knowledge of the test model wall temperature, boundary layer edge temperature (approximated by free stream value), the reservoir temperature and local temperature, an estimate of the local velocity (normalized to the edge value which is taken as the free stream value) can be made.

References

G-1 Coleman, E. R.; "Preliminary Analysis of Frontal Flow Field", Bendix Systems Division; FS-62TN-1020, January 1962.

APPENDIX H

CHEMICAL REACTIONS, RATE EQUATIONS, AND REACTION RATE CONSTANTS FOR KINETICS STUDY

The chemical reactions given below are considered representative of the reacting system to be considered in the kinetics experiment. The data have been previously published [H-1, H-2], and are presented here for convenience. The first set of equations defines the reactions of the system. The second set expresses the rate of formation of the various species. The specific reaction rate constants, gathered from various sources [H-3, H-4, H-5] are presented in tabular form.

A) Reactions

1. $Cs^+ + e + M \underset{k_2}{\overset{k_1}{\rightleftharpoons}} Cs + M$

2. $Cs_2^+ + e \underset{k_4}{\overset{k_3}{\rightleftharpoons}} 2Cs$

3. $O_2 + e + M \underset{k_6}{\overset{k_5}{\rightleftharpoons}} O_2^- + M$

4. $N_2 + Cs^+ + e \underset{k_8}{\overset{k_7}{\rightleftharpoons}} 2N + Cs$

5. $2N + NO \underset{k_{10}}{\overset{k_9}{\rightleftharpoons}} N_2 + NO^+ + e$

6. $2O + M \underset{k_{12}}{\overset{k_{11}}{\rightleftharpoons}} O_2 + M$

7. $2N + M \underset{k_{14}}{\overset{k_{13}}{\rightleftharpoons}} N_2 + M$

8. $N + O + M \underset{k_{16}}{\overset{k_{15}}{\rightleftharpoons}} NO + M$

9. $N + NO \underset{k_{18}}{\overset{k_{17}}{\rightleftharpoons}} N_2 + O$

10. $N + O_2 \underset{k_{20}}{\overset{k_{19}}{\rightleftharpoons}} NO + O$

B) Rate Equations

1. $\frac{d(e)}{dt} = -k_1 (Cs^+)(e)(M) + k_2(Cs)(M)$
$-k_3 (Cs_2^+)(e) + k_4(Cs)^2$
$-k_5 (O_2)(e)(M) + k_6(O_2^-)(M)$
$-k_7 (N_2)(e)(Cs^+) + k_8(N)^2 (Cs)$
$-k_{10} (N_2)(e)(NO^+) + k_9 (N)^2(NO)$

2. $\frac{d(Cs^+)}{dt} = -k_1 (Cs^+)(e)(M) + k_2 (Cs)(M)$
$-k_7 (N_2)(Cs^+)(e) + k_8 (N)^2 (Cs)$

3. $\frac{d(Cs)}{dt} = +k_1 (Cs^+)(e)(M) - k_2 (Cs) (M)$
$+2k_3 (Cs_2^+)(e) - 2k_4 (Cs)^2$
$+ k_7 (N_2)(Cs^+)(e) - k_8 (N)^2(Cs)$

4. $\frac{d(Cs_2^+)}{dt} = -k_3 (Cs_2^+)(e) + k_4(Cs)^2$

5. $\frac{d(N_2)}{dt} = -k_7 (N_2)(Cs^+)(e) + k_8 (N)^2 (Cs)$
$+k_9 (N)^2 (NO) - k_{10} (N_2) (NO^+)(e)$
$+k_{13} (N)^2(M) - k_{14} (N_2)(M)$
$k_{17} (N)(NO) - k_{18} (N_2)(O)$

$$6.\ \frac{d(N)}{dt} = 2k_7(N_2)(C\overset{+}{s})(e) - 2k_8(N)^2(Cs)$$
$$-2k_9(N)^2(NO) + 2k_{10}(N_2)(\overset{+}{NO})(e)$$
$$-2k_{13}(N)^2(M) + 2k_{14}(N_2)(M)$$
$$-k_{15}(N)(O)(M) + k_{16}(NO)(M)$$
$$-k_{17}(N)(NO) + k_{18}(N_2)(O)$$
$$-k_{19}(N)(O_2) + k_{20}(NO)(O)$$

$$7.\ \frac{d(NO)}{dt} = -k_9(N)^2(NO) + k_{10}(N_2)(\overset{+}{NO})(e)$$
$$+k_{15}(N)(O)(M) - k_{16}(NO)(M)$$
$$-k_{17}(N)(NO) + k_{18}(N_2)(O)$$
$$+k_{19}(N)(O_2) - k_{20}(NO)(O)$$

$$8.\ \frac{d(\overset{+}{NO})}{dt} = k_9(N)^2(NO) - k_{10}(N_2)(\overset{+}{NO})(e)$$

$$9.\ \frac{d(O_2)}{dt} = -k_5(O_2)(e)(M) + k_6(O_2^-)(M)$$
$$+k_{11}(O)^2(M) - k_{12}(O_2)(M)$$
$$-k_{19}(O_2)(N) + k_{20}(NO)(O)$$

$$10.\ \frac{d(O_2^-)}{dt} = k_5(O_2)(e)(M) - k_6(O_2^-)(M)$$

$$11.\quad \frac{d(O)}{dt} = -2k_{11}(O)^2(M) + 2k_{12}(O_2)(M) - k_{15}(N)(O)(M) + k_{16}(NO)(M) + k_{17}(N)(NO) - k_{18}(N_2)(O) + k_{19}(N)(O_2) - k_{20}(NO)(O)$$

$$12.\quad \frac{d(M)}{dt} = 0$$

The reaction rate constants are of the form

$$k_i = a_i T^{-b_i} e^{-C_i/T}, \text{ where}$$

i	a_i	b_i	C_i
1	$5. \times 10^{-26}$	1.0	0
2	1.25×10^{-10}	0	45200
3	1.6×10^{-2}	1.5	0
4	1.18×10^{-10}	1.5	33000
5	1.2×10^{-28}	0.5	0
6	1.58×10^{-13}	-1.0	5340
7	4.58×10^{-22}	1.5	68070
8	$1. \times 10^{-31}$	0	0
9	$1. \times 10^{-29}$	0	0
10	1.08×10^{-19}	1.5	5880
11	1.30×10^{-30}	1.0	0
12	9.07×10^{-4}	1.5	59480
13	9.22×10^{-27}	1.5	0
14	1.02×10^{-1}	1.5	113250
15	3.97×10^{-28}	1.5	0
16	9.25×10^{-4}	1.5	75500
17	1.72×10^{-11}	0	0
18	8.3×10^{-11}	0	37900
19	1.68×10^{-12}	-0.5	3120
20	5.07×10^{-10}	0	19140

References

H-1 Kresse, A. O.; "Equations and Data for Calculation of Electron Recombination Kinetics in $CsNO_3$-Al Reaction"; Bendix Systems Division; FS-61TN-1012, 1 November 1961.

H-2 Bendix Systems Division; "Semi-Annual Report - Preliminary Design Evaluation Decoy Ionization Trail Augmentation Studies"; 2 January 1962 (Secret).

H-3 Gerhauser, J. M.; "Cesium for Wake Seeding", Bendix Systems Division: RN37; 30 June 1961.

H-4 Coleman, E. R., and Doody, P. J.; "On Chemical Processes in Sypersonic Shock Layers"; Bendix Systems Division; BSR 509, March 1961.

H-5 Gatz, C. R., Rosser, W. A., and Smith, F. T.; "Study of Radar Beam Attenuation Rocket Exhaust Gases"; Stanford Research Institute; AFBMD-TR-61-39; February 1961.

APPENDIX I

ANALYSIS OF RADIATION FOR CHEMICAL RATE DATA

Since the major object of the planned experiments is the evaluation of the magnitude of the chemical kinetics it is necessary that the method of data analysis for chemical rates be described in some detail.

In what follows it is assumed that the concentrations of the important species can be measured to the desired accuracy. The accuracy actually obtainable is discussed elsewhere.

The major assumptions are:

1. The thermodynamic state-of-the-nozzle flow is known a priori implying:

   a. The flow is near frozen or near equilibrium and the deviations from either of these conditions do not significantly alter the thermodynamic state, or,

   b. The reactants are present in sufficient dilution such that they do not effect the thermodynamic parameters regardless of the extent of the reaction and an ideal gas law may be used.

2. The reactions given in Appendix H adequately describe the system.

3. The isothermal rate expressions are sufficiently accurate for the generation terms.

The basic equation is the specie continuity equation, which can be written in the absence of diffusion as:

$$\frac{dC_i}{dt} - \frac{C_i}{\gamma - 1} \frac{d}{dt} (\ln T) = \frac{\delta C_i}{\delta t} \qquad \text{(I-1)}$$

where

C_i = concentration of the i^{th} specie, $\frac{\text{number}}{cc}$

T = local temperature, ^{o}K

t = time, seconds

γ = isentropic exponent

$\frac{\delta C_i}{\delta t}$ = local rate of production of i^{th} specie due to reaction

= 0 for frozen flow

For equilibrium flow $\frac{\delta C_i}{\delta t} \neq 0$ (as is the case for isothermal equilibrium). The production of species equilibrium nozzle flow is due entirely to the temperature dependence of the equilibrium constant, i.e., for the reaction.

$$e^- + A^+ \rightarrow A \qquad \text{(I-2)}$$

the rate of depletion of electrons due to equilibrium expansion is

$$\frac{\delta \ln C_{e^-}}{\delta t} = -\frac{1}{2} \frac{d}{dt} \left(\ln \bar{K}_e \right) \frac{dT}{dt} \qquad \text{(I-3)}$$

It should be noted that similar terms should be included in the near frozen calculations. However, under the near frozen assumption, it is implied that the rate of change of concentration due to reaction is small compared to the change due to expansions. This allows the use of isothermal form of the rate equations. In any case, the accuracy of any kinetics experiment does not warrant consideration of what are essentially second order terms in the Taylor expansion of the rate of production except near equilibrium where the first order terms are zero.

Returning to Equation (I-1) and assuming that the right hand side is adequately represented by the isothermal rate of production as given in Appendix H we may write for the general case a set of 11 equations of the

form given in (I-1) corresponding to the 11 reacting species. The unknowns are the 10 rate constants of the ten stoichiometric chemical equations. This implies that the eleven equations are not independent and in fact they are not since by charge conservation we have

$$\frac{\delta(e)}{\delta t} - \frac{\delta(C_s^+)}{\delta t} - \frac{\delta(Cs_2^+)}{\delta t} - \frac{\delta(NO^+)}{\delta t} + \frac{\delta(O_2^-)}{\delta t} = 0 \qquad \text{(I-4)}$$

Thus any one of the conservation equations corresponding to the terms in (I-4) may be eliminated from the set of simultaneous equations and used later as a consistency check.

The measured quantities in the experimental set up are the specie concentrations at several positions in the nozzle. In practice, this is done by making the measurements at the exits of a family of nozzles related as shown in the sketch.

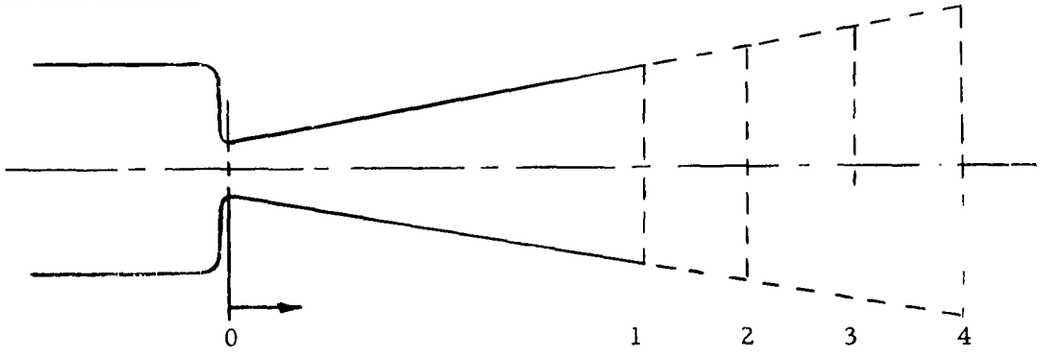

Equation (I-1) may be transformed to space coordinates by

$$\frac{dx}{v} = dt$$

$$v\,\frac{dC_i}{dx} - \frac{C_i\,v}{\gamma - 1}\,\frac{d}{dx}(\ln T) = \frac{\delta C_i}{\delta t} \qquad \text{(I-5)}$$

Assuming that v and T are predetermined functions of x and all the C_i are determined experimentally as a function of x, the left hand side of (I-5) is determined for every point of the nozzle. Thus the right hand side of (I-5) forms a set of linear simultaneous algebraic equations in the unknown rate constants for every point along the axis of the nozzle and hence for the range of temperatures encountered in the nozzle. The specific rate constants may be solved for, plotted versus temperature in the usual way, and analyzed for the exponential and pre-exponential factors by well established methods.

Intrinsically the method of analysis is simple and correct. However, there are two difficulties which are likely to be encountered; one numerical and one physical.

The numerical source of error is in the left hand side of (I-5) which is essentially the difference of two slopes; i.e., the total rate of change of concentration and the rate of change due to the expansion process. Near frozen flow these slopes are nearly equal, leading to the small difference of large numbers.

Related to this, but inherent in the diagnostic instrumentation, is the accuracy with which the concentrations can be determined.

Depending upon the specific results of the experiment it may be necessary to use a finite difference form of (I-5) over a substantial nozzle segment, in which case a detailed correlation with temperature is no longer possible. For recombination reactions this defect is slight since the temperature dependence is usually a small power of T rather than exponential. It is, however, just the recombination reactions which are most interesting for the present problem.

APPENDIX J

PHYSICAL DATA

It is the purpose of this appendix to set down in one place as much of the required physical data as possible, in order to facilitate the reduction of experimental data. The following material has been obtained from many sources (J-1, J-2, J-3, J-4), and includes constants, conversion factors, and spectroscopic data for the species expected to be present in the gases analyzed.

1) Physical Constants

h = Planck's constant = 6.6251×10^{-27} erg-sec.

c = Light velocity = 2.9978×10^{10} cm/sec

k = Boltzmann's constant = 1.3805×10^{-16} erg/^{o}K

c_1 = First radiation constant = $2\pi hc^2$

= 3.7402×10^{-5} erg-cm^2/sec

c_2 = Second radiation constant = hc/k

= 1.4388 cm - ^{o}K

e = Electronic charge = 4.8025×10^{-10} esu

A_o = Avogadro's number = 6.0228×10^{23} particles/mole

2) Energy Conversion Factors

	erg	cm^{-1}	electron volt
erg	1	5.0358×10^{15}	6.2421×10^{11}
cm^{-1}	1.98258×10^{16}	1	1.2395×10^{-4}
electron volt	1.60203×10^{-12}	8067.5	1

3) Spectroscopic Data

A) Atomic Specie

i) Nitrogen and Oxygen

The following spectral lines due to atomic oxygen and nitrogen may be observed:

Oxygen	Nitrogen
4370 Å	4110 Å
5330	4150
6160	6010
6460	6480
7770	6640
7950	6720
8220	
8230	
8450	

ii) Aluminum, Sodium, and Potassium

The most intense lines for each element are given, together with the transition involved, the transition probability, and the energy level and degeneracy of the upper state.

Transition	λ(Å)	A(sec^{-1})	g	E(cm^{-1})
Aluminum				
$3d\ ^2D5/2 \rightarrow 3p\ ^2P3/2$	3092.71	6.95×10^7	6	32436.79
$4s\ ^2S1/2 \rightarrow 3p\ ^2P3/2$	3961.53	2.21×10^7	2	25347.69
Sodium				
$4p\ ^2P3/2 \rightarrow 3s\ ^2S1/2$	3302.32	3.78×10^6	4	30272.51
$3p\ ^2P3/2 \rightarrow 3s\ ^2S1/2$	5889.95	9.04×10^7	4	16973.38
$3d\ ^2D5/2 \rightarrow 3p\ ^2P3/2$	8194.81	1.39×10^7	6	29172.86

Potassium

$6p\ ^2P3/2 \rightarrow 4s\ ^2S1/2$	3446.72	7.32×10^5	4	29007.70
$5p\ ^2P3/2 \rightarrow 4s\ ^2S1/2$	4044.14	3.01×10^6	4	24720.20
$4p\ ^2P3/2 \rightarrow 4s\ ^2S1/2$	7664.91	5.57×10^7	4	13042.89

iii) Cesium

The first table is similar in all respects to the preceeding one, i.e., transition, wavelength, probability, degeneracy, and energy are given. The second table presents the Stark broadening data of Griem. (D-1) The data is in the form of half-widths of the specified line (in Å) for an electron density of 10^{16} cm^{-3} at two temperatures.

Transition	λ(Å)	A(sec^{-1})	g	E(cm^{-1})
$9p\ ^2P3/2 \rightarrow 6s\ ^2S1/2$	3611.52	3.49×10^5	4	27681.96
$9p\ ^2P1/2 \rightarrow 6s\ ^2S1/2$	3617.41	2.35×10^4	2	27637.29
$8p\ ^2P3/2 \rightarrow 6s\ ^2S1/2$	3876.39	1.54×10^6	4	25791.78
$8p\ ^2P1/2 \rightarrow 6s\ ^2S1/2$	3888.65	5.52×10^5	2	25709.14
$7p\ ^2P3/2 \rightarrow 6s\ ^2S1/2$	4555.35	4.82×10^6	4	21946.66
$7p\ ^2P1/2 \rightarrow 6s\ ^2S1/2$	4593.18	2.06×10^6	2	21765.65
$8d\ ^2D3/2 \rightarrow 6p\ ^2P1/2$	6012.14	3.47×10^5	4	27811.25
$8d\ ^2D5/2 \rightarrow 6p\ ^2P3/2$	6214.81	1.54×10^6	6	27822.94
$8d\ ^2D3/2 \rightarrow 6p\ ^2P3/2$	6219.33	1.71×10^5	4	27811.25
$7d\ ^2D3/2 \rightarrow 6p\ ^2P1/2$	6725.12	1.42×10^6	4	26047.86
$7d\ ^2D5/2 \rightarrow 6p\ ^2P3/2$	6975.21	2.63×10^6	6	26068.83
$7d\ ^2D3/2 \rightarrow 6p\ ^2P3/2$	6985.43	2.92×10^5	4	26047.86
$6p\ ^2P3/2 \rightarrow 6s\ ^2S1/2$	8521.10	4.85×10^7	4	11732.35
$6d\ ^2D3/2 \rightarrow 6p\ ^2P1/2$	8761.38	2.80×10^6	4	22588.89
$6p\ ^2P1/2 \rightarrow 6s\ ^2S1/2$	8943.50	2.84×10^7	2	11178.24
$6d\ ^2D5/2 \rightarrow 6p\ ^2P3/2$	9172.24	7.00×10^6	6	22631.83

Transition	Half-Width (Å) 2500 °K	5000 °K
$7p\ ^2P3/2 \rightarrow 6s\ ^2S1/2$	0.205	0.274
$7p\ ^2P1/2 \rightarrow 6s\ ^2S1/2$	0.168	0.208
$8p\ ^2P3/2 \rightarrow 6s\ ^2S1/2$	0,613	0.718
$8p\ ^2P1/2 \rightarrow 6s\ ^2S1/2$	0.491	0.593
$9p\ ^2P3/2 \rightarrow 6s\ ^2S1/2$	1.12	1.34
$9p\ ^2P1/2 \rightarrow 6s\ ^2S1/2$	1.21	1.44
$7d\ ^2D3/2 \rightarrow 6p\ ^2P1/2$	1.30	1.63
$7d\ ^2D3/2 \rightarrow 6p\ ^2P3/2$	1.40	1.76
$7d\ ^2D5/2 \rightarrow 6p\ ^2P3/2$	1.32	1.69
$8d\ ^2D3/2 \rightarrow 6p\ ^2P1/2$	3.02	3.66
$8d\ ^2D3/2 \rightarrow 6p\ ^2P3/2$	3.23	3.92
$8d\ ^2D5/2 \rightarrow 6p\ ^2P3/2$	3.05	3.77
$9p\ ^2P3/2 \rightarrow 5d\ ^2D3/2$	6.73	7.70

iv) Hydrogen

This section presents the required spectroscopic data, including Stark Coefficients, for the first three lines of the Balmer Series of the hydrogen atom, i.e., H_α, H_β, and H_γ.

The first-order Stark Coefficients are taken from Condon and Shortley [J-13], and are given in Angstrom units per kilovolt/cm. It should be noted here, that the data of Condon and Shortley do not apply to the usual eigenfunctions, characterized by the quantum numbers n, l, m, in a spherical coordinate system. Rather, a parabolic coordinate system is employed, characterized by the quantum numbers k_1, k_2, m.

Here
$$n = k_1 + k_2 + |m| + 1 \qquad \text{(J-1)}$$

and n and m have the same significance as in the spherical case. According to Schiff [J-5], the eigenfunctions in one system are linear combinations of the eigenfunctions in the other system.

Thus, since the Stark data is given for transitions between states having eigenfunctions based on the parabolic coordinate system, a consistent set of transition probabilities must be determined. The transition probability is given by

$$A^{nm} = \frac{64 \epsilon^2 c^3 \pi^4}{3 h \lambda^3} R^{nm} R^{mn} = 2.025 \times 10^{18} \frac{1}{\lambda^3} S \qquad \text{(J-2)}$$

where S is the line strength of the transition expressed in units of $\epsilon^2 a_o^2$ and λ is given in Angstrom units. Thus

$$S = \epsilon^2 \, R^{nm} \, R^{mn}$$

$$= \epsilon^2 \left[\int \psi_n \, \psi_m^* \, x \, d\tau \int \psi_m \, \psi_n^* \, x \, d\tau \right. \qquad \text{(J-3)}$$

$$+ \int \psi_n \, \psi_m^* \, y \, d\tau \int \psi_m \, \psi_n^* \, y \, d\tau$$

$$\left. + \int \psi_n \, \psi_m^* z \, d\tau \int \psi_m \, \psi_n^* \, z \, d\tau \right]$$

Here the ψ_n and ψ_m are the eigenfunctions of the two states involved in the transition, and the asterisk indicates the complex conjugate. The expressions for x, y, z, $d\tau$ and ψ are found in Condon and Shortley.

The first table below gives the wave length in Å, and upper state energy [J-7], in cm^{-1}, for the three lines of the Balmer Series considered. The second table gives the transition probability, in reciprocal seconds, and the first-order Stark coefficient, in Å per kilovolt/cm, for each specific transition characterized by k_1, k_2, m.

Line	Wave length	Upper State Energy
H_α	6562.85	97492.
H_β	4861.33	102824.
H_γ	4340.47	105292.

H_α line (n = 3 to n = 2)

Transition	Probability ($\times 10^{-8}$)	Stark Coefficient
110-010	.0858	.0555
101-001	.162	.0833
200-100	.235	.1108
002-001	.648	0.
110-001	.0124	0.
101-100	.272	.0277

H_β line (n = 4 to n = 2)

Transition	Probability ($\times 10^{-8}$)	Stark Coefficient
210-010	.0663	.0914
201-001	.0513	.1218
300-100	.00962	.1523
111-010	.00480	.0304
102-001	.103	.0609
210-001	.0203	.0609
201-100	.00786	.0914

H_γ line (n = 5 to n = 2)

Transition	Probability ($\times 10^{-8}$)	Stark Coefficient
220-010	.00548	.0243
211-001	.00337	.0607
310-010	.0694	.1458
301-001	.0109	.1882
400-100	.0462	.2185
112-001	.0403	0.
220-001	.00928	0.
211-100	.000399	.0364
202-001	.0269	.1217
310-001	.193	.1217
301-100	.0299	.1581

B) Molecular Specie

There will be at least three band spectra, due to molecular constituents of the rocket motor exhaust, appearing in the wavelength region of interest. The higher vibrational transitions of the first positive band of nitrogen, as well as the second positive band of nitrogen, and a band in the near infrared due to oxygen should be encountered. The data below give the transitions involved, the locations of the band heads, and the molecular spectroscopic constants.

Nitrogen

First Positive

$\lambda_{oo} = 10470\ \text{Å}$

$B\ {}^3\Pi_g \rightarrow A\ {}^3\Sigma_u^+$

Second Positive

$\lambda_{oo} = 3370\ \text{Å}$

$C\ {}^3\Pi_u \rightarrow B\ {}^3\Pi_g$

State	$T(cm^{-1})$	$\omega_e(cm^{-1})$	$\omega_e x_e(cm^{-1})$	$B_e(cm^{-1})$	$\alpha_e(cm^{-1})$
$C\ {}^3\Pi_u$	89147.	2035.1	17.08	1.8259	0.0197
$B\ {}^3\Pi_g$	59626.	1734.11	14.47	1.6380	0.0184
$A\ {}^3\Sigma_u^+$	50206.0	1460.37	13.891	1.440	0.013

Oxygen

$\lambda_{oo} = 7620\ \text{Å}$

$b\ {}^1\Sigma_g^+ \rightarrow X\ {}^3\Sigma_g^-$

State	$T(cm^{-1})$	$\omega_e(cm^{-1})$	$\omega_e x_e(cm^{-1})$	$B_e(cm^{-1})$	$\alpha_e(cm^{-1})$
$b\ {}^1\Sigma_g^+$	13195.222	1432.687	13.9500	1.40041	0.01817
$X\ {}^3\Sigma_g^-$	0	1580.361	12.0730	1.44566	0.01579

REFERENCES

J-1 Doody, P.J., and Santomieri, J., "Thermal Emission of Neutral Cesium", Bendix Systems Division; FS-61TN-1015; 16 November 1961.

J-2 Herzberg, G., Spectra of Diatomic Molecules; Van Nostrand; New York, 1950.

J-3 Condon, E. V., and Shortley, G. H., Theory of Atomic Spectra; Cambridge, 1957.

J-4 Hodgman, C. D., (ed); Handbook of Chemistry and Physics, (41 st Ed); Chemical Rubber Publishing Company, Cleveland, Ohio, 1959.

J-5 Schiff, L. I.; Quantum Mechanics; McGraw-Hill, 1955.

J-6 Herzberg, G.; Atomic Spectra and Atomic Structure; Dover Publ.; 1944.

J-7 Moore, C. E.; Atomic Energy Levels; NBS Circular 467; 1949.